CONSEQUENCE ANALYSIS OF THE ACCIDENTAL RELEASE OF SUPERCRITICAL CO_2 FROM HIGH PRESSURE PIPELINES

By

PREETI JOSHI

Bachelor of Technology - Chemical Engineering

Osmania University

Hyderabad, Telangana

2011

Submitted to the Faculty of the
Graduate College of the
Oklahoma State University
in partial fulfillment of
the requirements for
the Degree of
MASTER OF SCIENCE
July, 2016

CONSEQUENCE ANALYSIS OF THE ACCIDENTAL RELEASE OF SUPERCRITICAL CO_2 FROM HIGH PRESSURE PIPELINES

Thesis Approved:

Dr. Qingsheng Wang

Thesis Adviser

Dr. Prem Bikkina

Dr. Clint Aichele

ACKNOWLEDGEMENTS

I cannot call this thesis the output of my hard work without acknowledging all those people who have contributed to making it possible and who made my graduate experience worthwhile.

I would like to express my deepest gratitude to my advisor, Dr. Qingsheng Wang, for his constant guidance, support and encouragement throughout my research. I am very grateful to have a mentor like him, who gave me freedom to explore my own ideas and provided necessary mentoring when required with his expertise and ideas to get meaningful results.

Besides my advisor, I would also like to sincerely thank Dr. Prem Bikkina and Dr. Clint Aichele for serving on my committee and taking time off their busy schedule to provide valuable insight and feedback for sorting out the technical details of my work.

I am grateful to all the faculty and staff of the Department of Chemical Engineering at Oklahoma State University for their support and encouragement.

Most importantly, this work wouldn't have been possible without the love and support of my family. I would like to express my heart-felt gratitude to my parents, Mrs. Mangala Joshi and Mr. Amrut Joshi who have supported me all through this journey. Last but not the least, none of this would have been possible without the love and encouragement of my husband, Mr. Mandar Bhilegaonkar, who has always believed in me and guided me constantly in making this research experience substantive.

Name: PREETI JOSHI

Date of Degree: JULY, 2016

Title of Study: CONSEQUENCE ANALYSIS OF THE ACCIDENTAL RELEASE OF SUPERCRITICAL CO_2 FROM HIGH PRESSURE PIPELINES

Major Field: CHEMICAL ENGINEERING

Abstract: Climate change and global warming is a major challenge that we are facing today which involves the emission of harmful greenhouse gases into the atmosphere. CO_2 is one of the primary greenhouse gases, among others, which is majorly as a result of anthropogenic emissions. Carbon capture and storage (CCS) is an integrated technology that prevents large amounts of CO_2 from entering the atmosphere by capturing it from large point sources and safely sequestering them in geological storages. Safe transportation of the captured CO_2 through long distance pipelines is a challenge that we face today due to the lack of technology to properly address the knowledge gap at various operating conditions. Pressurized pipelines are considered to be the most efficient and reliable way to transport CO_2 due to the high density and low viscosity of CO_2. Any accidental discharge from such high pressure pipelines may result in a significant damage to the ambient atmosphere and it also poses a dominant threat to human health. Therefore, transportation safety of CO_2 should clearly be one of the most critical process design considerations in carbon-capture and storage (CCS) area. It is important to understand the unusual phase transition behavior of CO_2 in order to model the fluid dynamics and subsequent atmospheric dispersion during such an accidental release. This thesis deals with a two-step approach for computing the final pollutant concentration. In the first step, the release rates of supercritical CO_2 are calculated due to sudden decompression at the leak which may lead to chocked flow conditions. These release rates would serve as the key parameter in the second step, dispersion modeling, which determines the toxic concentration levels of CO_2 at various downwind distances. Computational Fluid Dynamics software, Ansys Fluent 16.2 version is used for predicting the jet release rates and the concentration variations of pure CO_2 over a given period of time and distance. The Fluent model has been validated against experimental work carried out by BP's DF1 project at the Spadeadam site (UK) involving transient horizontal releases of supercritical CO_2. A further investigation was carried out to study the impact of CO_2 dispersion in the presence of obstacles such as buildings. This consequence model would not only be helpful to predict and control the harmful release of CO_2 in ambient air, but would also serve as a hazard design tool for determining the minimum safe distances to populated areas and planning emergency response and evacuation procedures in case of pipeline leakage.

TABLE OF CONTENTS

LIST OF TABLES

Table Page

LIST OF FIGURES

Figure Page

CHAPTER I

INTRODUCTION

1.1 Background

Carbon dioxide (CO_2) is a major greenhouse gas and its concentration in the atmosphere has increased significantly in the past century primarily due to human activities such as burning fossil fuels and industrial emissions. Its emission has rapidly increased in the last 50 years reaching to a concentration of almost 9500 $MMTCO_2$ in 2011 (Boden, Marland et al. 2015) and the average estimated increase in the global CO_2 emissions every year is almost 1.1% (IEA 2010). The increase in these global emissions can cause the melting of snow caps which eventually leads to the rise of the sea levels and drastic climatic changes.

CO_2 emissions in the United States have drastically increased over the past two decades to about 9% from 1990 to 2014. Majority of this can be attributed to the anthropogenic emissions, primarily from the burning of fossil fuels for energy generation. The following figure shows the increasing trend of CO_2 emissions in the last few decades.

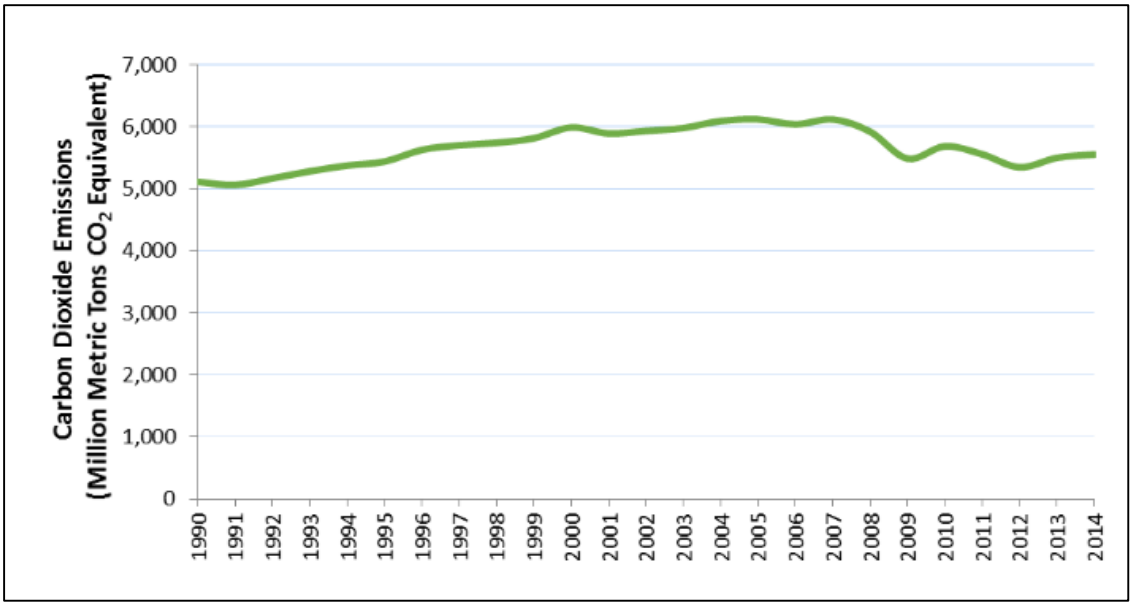

Figure 1: Increasing trend of CO_2 emissions (U.S. Environmental Protection Agency 2016)

Carbon Capture and Storage (CCS) is identified as the most promising technologies for significant reduction in the CO_2 emissions in the atmosphere. In this process, the concentrated CO_2 is captured from the source such as a gas processing plant, instead of releasing it to the atmosphere, and transported through pipelines before it reaches the geological sink or used in enhanced oil recovery (EOR) process. When the source emitting CO_2 is not directly located above the storage site, transportation is required. For small volumes of CO_2, ships or others offshore options are economical. But for transporting large volumes of CO_2, the most cost effective way would be through pipelines. Today CO_2 pipelines extend to more than 2500 km in the western part of USA and carry over 50 $MTCO_2$ per year from natural gas resources and supply it for EOR purposes in west Texas and other places (IPCC). Pressurized pipelines are thus considered to be the most efficient way for transporting large volumes of CO_2 especially when the storage site is located at long distances from the emission source.

It is estimated that pipeline deployment could be in the order of 10,000-12,000 km in the next ten years (to transport 300 $MTCO_2$ from 100 CCS projects), 70,000-120,000 km by 2030, and 200,000-360,000 km by 2050, with investment in the order of $0.5-1 trillion in United States,

Europe and China (IEA 2010). This would invite additional necessity for designing safe transportation means of CO_2 in accordance with appropriate standard design and operation codes.

Risk analysis for safe transportation through populated areas should be taken into consideration for designing an appropriate route for the pipeline. Acceptable risk is determined based on the amount of human activity in a particular area of the route. For determining risk basis, identifying the frequency and the possible aftermath of such hazards is important. Practically, pipelines cannot be deviated much from the actual routes due to economic constraints. Maintaining proper balance between the risk factor and cost of the pipeline, by avoiding the risky areas like suburbs or valleys where dense CO_2 can accumulate, forms an important decision in pipeline routing. Maintaining pipeline integrity by adhering to the design standards like selecting the appropriate material of construction, nominal pipe size etc., at the same time selecting an optimal route should be all taken into consideration for effectively designing the pipeline.

1.2 Specific Properties of CO_2

CO_2 is a colorless and odorless gas which if present above certain concentrations in air poses risk to human health (usually above 50,000 ppm) (NIOSH 1996). At standard temperature of 273.15 K (0 ^oC) and pressure of 101.325 KPa (1 atm), CO_2 has a density of 1.98 kg/m^3 which is almost 1.5 times that of air (1.2754 kg/m^3). This may cause CO_2 to accumulate in low lying areas in the event of a pipeline leak posing serious threat to the surrounding population. Hence, special care must be taken to the pipeline transportation that pass through populated areas.

CO_2 exists in all 4 phases: gas, liquid, solid and supercritical. From the phase diagram below, we can see that the critical pressure and temperature of CO_2 is 7.38 MPa (73.8 bar) and 304.25K (31.1 ^0C). Above this temperature and pressure, CO_2 acts as a supercritical fluid which has more liquid like density but has other properties like diffusivity and viscosity like that of vapor. This makes it suitable for economical transportation of CO_2 in this state.

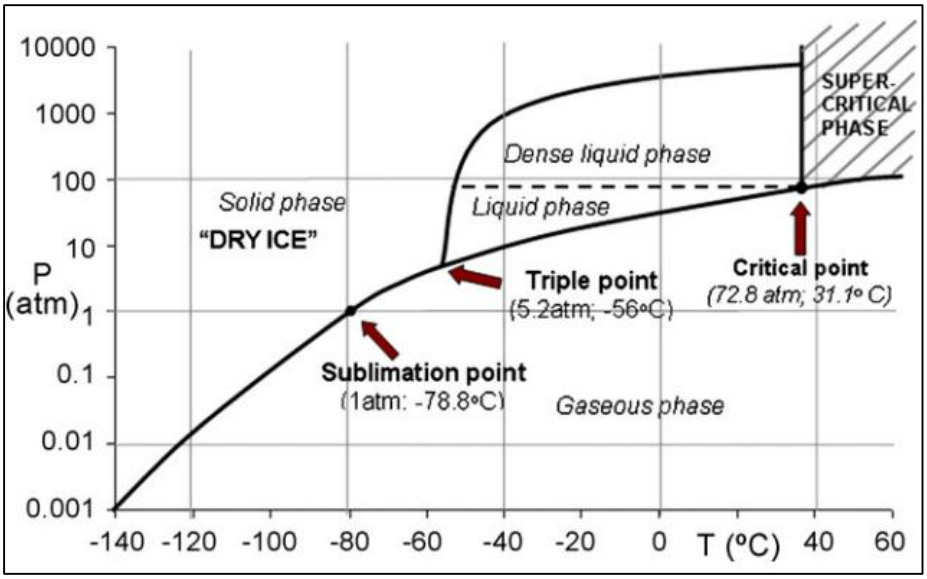

Figure 2: Phase diagram for CO_2 (Mazzoldi, Hill et al. 2008)

The various physical and chemical properties of CO_2 are tabulated below in the form of a table:

Table 1: Specific properties of CO_2 (Henning 2013)

Property	Value
Appearance and Odor	Colorless and Odorless; sharp nasal sensation at high concentration
Molecular weight	44.01 g/mol
Critical Pressure	7.38 MPa (73.8 bar)
Critical Temperature	304.25K (31.1 ^oC)
Triple point	0.518 MPa (5.18 bar) at 216.55 K (-56.6 K)
Standard gas density	1.98 kg/m^3
Density at critical point	467 kg/m^3
Liquid density at 0 ^oC, 70 bar	995 kg/m^3
Solid density at freezing point	1562 kg/m^3
Sublimation temperature, 1 bar	197.5 K (-78.5 ^0C)

From the above conditions, we can see that the triple point pressure of CO_2 is 5.18 bar which is much above the atmospheric pressure conditions. Hence, at atmospheric pressure (1 bar)

and sublimation temperature (194.65 K or -78.5 ^{o}C), CO_2 exists only in gaseous and solid form (or dry ice) and directly sublimates from dry ice (solid) to gaseous phase.

1.3 Effect of Impurities on CO_2 Transportation

The resultant CO_2 captured could be due to the burning of fossil fuels or industrial processes. Depending upon the captured source, there can be large amount of combustion impurities such as H_2S, NO_x, SO_x or water vapor which have to be removed before they can be transported. CO_2 liquid has an increasing ability to dissolve water at enhanced pressures which is opposite to that of CO_2 vapor (DNV 2010). The presence of impurities could alter the ability of CO_2 fluid to dissolve water and hence, should be addressed properly. In a typical CCTS transportation, the water content should be reduced at the source before transportation to a desirable level of <500 ppm (Henning 2013). If water content exceeds this limit, it reacts with carbon dioxide to form carbonic acid as per the following reaction and this leads to corrosion of carbon steel pipelines. The removal of water is usually done by employing dehydration technology prior to transportation.

$$CO_2 + H_2O \longrightarrow H_2CO_3 \text{ (carbonic acid)} \qquad \textbf{(1.1)}$$

The presence of impurities impacts the physical properties of CO_2 by altering the density, critical pressure and temperature, thereby affecting the phase behavior. This in turn impacts the operating pressures of the pipeline and makes the leaking CO_2 more toxic as compared to pure CO_2. Correct equations of state such as Peng Robinson (PR) or Soave-Redlich Kwong (SRK) should be used to accurately predict the properties of the resulting mixture. The effect of impurities on the phase diagram of CO_2 is depicted in the figure below:

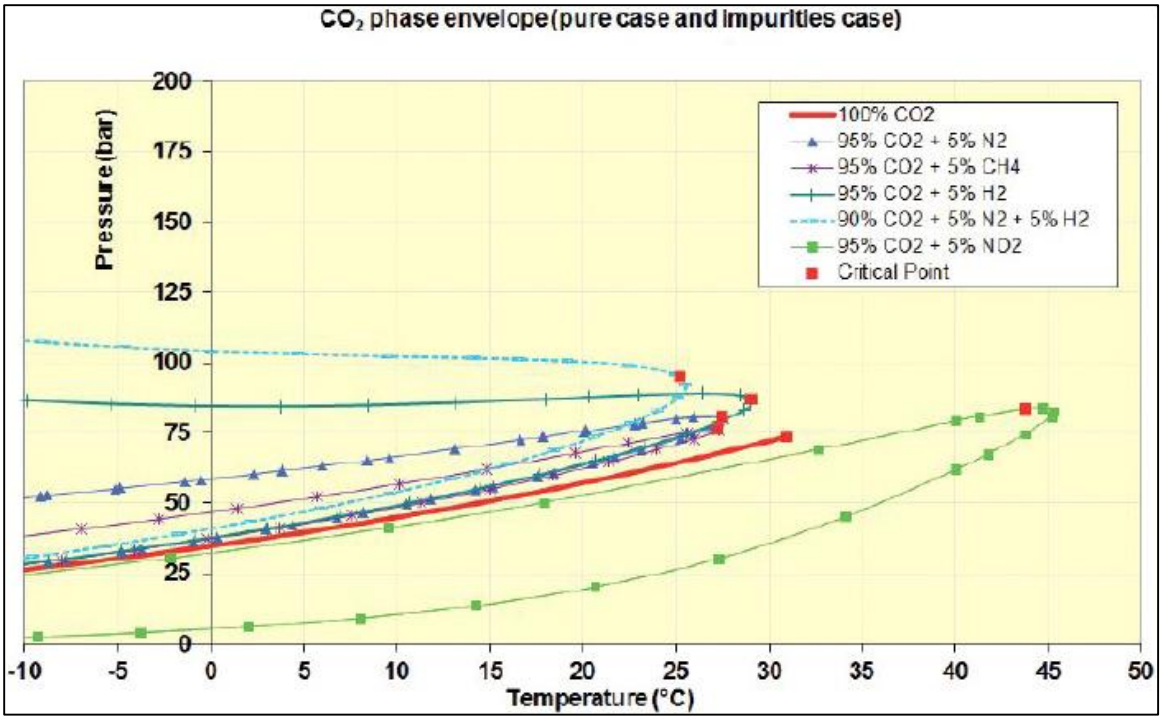

Figure 3: Effect of impurities on the phase diagram of CO_2 (Henning 2013)

One other important effect of the presence of impurities is that it would impact the prediction of the mass flow rate from the near-field dispersion modeling results. This would in turn impact the source term calculations which would serve as an input for dispersion modeling. The presence of impurities lowers the mass flow rate when compared to pure CO_2 case. Hence, to design a worst case scenario, pure CO_2 case can be considered.

In this study, 100% pure CO_2 has been considered for all design purposes. In other words, it is assumed that the impurities are so small that they do not affect the flow characteristics of CO_2.

1.4 Process of CO_2 Transportation

Pipelines have been used from a long time to transport a wide variety of fluids in large volumes such natural gas or even oil. CO_2 transportation through pipelines has evolved in the last few decades and is observed as the most common ways of transportation today. CO_2 from the industrial processes is separated from the other gases and compressed to a very high pressure before

it is transported. This is done to avoid the two-phase regime in order to facilitate cost economical pumping through longer distances.

The sequence of steps in the transportation of CO_2 from the source to the geological sink can be depicted by the following flow chart:

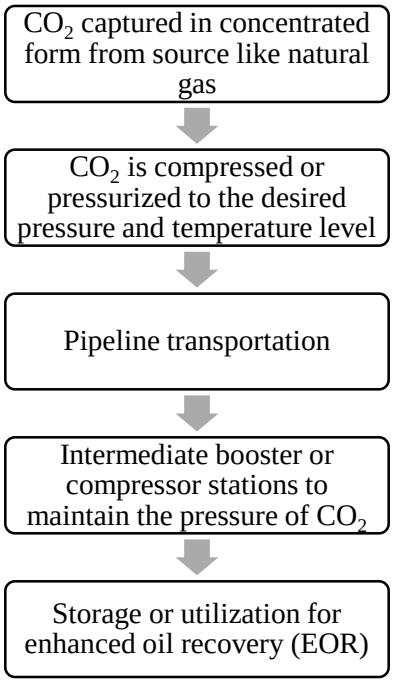

Figure 4: Sequence of steps in CO_2 transportation

1.5 Identification of Sources and Sinks of CO_2

Some of the common sources and sinks in the process of carbon capture and storage (CCS) technology are listed below in the form of a table:

Table 2: Common sources and sinks of CO_2

Common Sources of CO_2	**Common Sinks of CO_2**
Gas processing plants	Deep saline formations
Fossil-fueled power stations	Methane recovery
Natural sources of CO_2	Oil fields for EOR
	Depleted oil and gas fields

1.6 Operating Conditions for Transporting CO_2

1.6.1 Preference of Supercritical over Subcritical Transportation of CO_2

One of the important considerations in the optimum transportation of CO_2 through pipelines is the pipeline pressure. As discussed above, the most economical and efficient ways of transportation, especially for long distance pipelines, is by setting the pressure above the critical point. Usually, the decision of how much above the critical is decided by the delivery requirements at the sink. But an optimum injection pressure of the range of 10-15 MPa is common (Henning 2013).

Although CO_2 is transported in both sub-cooled ($P>P_c$ and $T<T_c$) and supercritical phase ($P>P_c$ and $T>T_c$) (also termed as dense phase), supercritical transportation above 8 MPa is preferred for long distances due to its density and stability. Other factors that determines the state and operating pressure of the pipeline is how the power requirement is distributed along the length of the pipeline. For a subcritical transportation, the power requirement would be maximum at the terminal (sink). While for the supercritical transportation, the power requirement is maximum at the emitters. The total power consumed at the emitters and the terminals by either subcooled or supercritical transportation would be almost the same but the main difference lies in the how the pressure drop is handled over the collection. The pressure drop over the entire pipeline shouldn't be too large. Hence for long distance pipelines, this would mean that in order to maintain adequate pressure for the liquid in subcooled state, there would be a requirement to either place booster stations at immediate intervals or to increase the pipeline sizes, both of which are not productive in terms of cost. The consecutive average distance between two booster pumps is 50 km as per Det Norske Veritas (DNV). On the other hand, operating the pipeline in supercritical state minimizes the cavitation problem at the booster stations and pumps and as a result, is easier and cost efficient for transportation (Witkowski, Rusin et al. 2015).

1.6.2 Types of Leakages

Determining the type of leak will help us model the release accurately and predict the resulting impact from each of the leakage scenarios. Depending upon the size and location of the leak, there can be a huge spectrum of leak phenomena that can be categorized. This can range from a small pinhole leak to a full-bore rupture. The different potential leak scenarios that have been categorized are:

Table 3: Hole-sizes and frequency analysis (McConnell and Haswell 2012)

Equivalent hole size	Number of incidents	Frequency (incidents per 1000 km/yr)
Full bore and above	7	0.009
110 mm-Full Bore	3	0.004
40 mm-110 mm	7	0.009
20 mm-40 mm	23	0.028
6 mm-20 mm	31	0.038
0-6 mm	114	0.140

The values mentioned for hole sizes in the table above correspond to the diameter of a circular hole. For non-circular leaks, the hole size is calculated by taking the area equivalent to the circular hole diameter area. Full-bore ruptures are ruptures with a size equal to the diameter of the pipeline, and are usually designed considering maximum damage or the worst case scenario. The frequency of failure resulting from a full-bore rupture is very low when compared to punctures and hence, in the present study, a circular hole-size of 11.94 mm diameter is considered in accordance with BP DF1 CO_2 experiments.

Release Angle:

Depending upon the direction of release, the scenarios can be briefly divided into 3 categories:

1. Vertical release or vent release: A vertically upward pointing leak is a high momentum jet release which quickly decompresses and entrains large amount of ambient air forming dry ice which gives it a white smoke like color. Most of the solids are sublimated within the jet due to the high frictional heating with the surrounding atmosphere without much of the plume reaching the ground. Hence, such a release is not found to cause excess damage to the surrounding population.
2. Downward impinged release: A downward pointing leak impinges the jet release directly on the ground forming large dry-ice bank which slowly sublimates with time. This can be dangerous as the solid dry ice persists for longer time causing long-lasting effects of toxic concentration levels in air.
3. Horizontal release: This is the most common and conservative type of release which poses maximum risk to the surrounding population. This is due to the fact that the high momentum jet is directly dispersed downwind which can cause serious threat in the presence of obstacles. Depending upon the size of the leak, dry ice may rainout on the ground which contributes to additional sources of CO_2 sublimating slowly with time.

Figure 5: Types of Leaks – (a) Vertical (b) Downward (Mazzoldi and Oldenburg February 2013), (c) Horizontal (Henning 2013)

All BP trials were horizontal releases and hence the present study deals with the horizontal release phenomena in which the leak direction is horizontal (parallel to the wind direction).

Buried or Above Ground:

Depending on the ways of transporting CO_2, pipeline transportation can be either

- buried or
- above the ground

While buried pipelines are safer means of transporting CO_2, it invites additional cost factors for preventing external corrosion which can be prevented either by cathodic protection or by external coating. Small leaks caused above ground can be detected while the same condition in buried pipelines may make the soil acidic by choosing the least resistance path. Careful assessment of the relative cost and the operational preferences should be done before choosing the method of transportation. In the present work, 'above the ground' transportation is considered with an altitude of 1.1 m above ground.

1.7 Risk Analysis

Risk analysis involves the frequency of occurrence of failure cases and reasons for those failures. Later in the section, the possible consequences are listed and their tolerance limits are described. Risk or hazard analysis is important from the perspective of dispersion modeling which requires topographical conditions of the surroundings and the density of population in the vicinity of the pipeline.

1.7.1 Reasons for Pipeline Failure and Past Failure Cases

Some of the major parameters that caused pipeline failures/ruptures in the past are presented below (HECA Project Site 2009):

- Equipment errors due to abnormal operation and maintenance of pipes, joints and valves (including third-party damage)
- Pipeline corrosion (can also be due to external conditions or poor maintenance)
- High pressure and temperature conditions
- Human errors (also includes violation of Occupational Safety and Health Administration (OSHA) workplace safety regulations)

1.7.2 Past Failure Cases Analysis:

The information to known incidents serves as a key tool in identifying what failure scenarios have occurred in the past and the reasons for their failure which would determine what possible events should be modeled to prevent the consequences of leak. This type of hazard analysis would also provide us the necessary information to the general mechanisms which lead to this type of failure and estimate the extent and the magnitude of such leaks. These risk analysis tools help us patch the loopholes that exist in systems safety and identify areas which are outside our experience and expertise which would eventually increase the effectiveness with which these hazards can be

managed. A brief information about the failure rates of CO_2 pipelines in the United States over the last couple of years and their associated failure modes have been quantified in the table below.

Table 4: History of failure rates of CO_2 pipelines (HECA Project Site 2009)

Failure mode	Total number of accidents between 1986 and 2008	Percentage	Historic failure rate (per mile of CO_2 pipeline per year)
Equipment Failure	6	46	7.77E-05
Corrosion	2	15.5	2.70E-05
Operation Error	2	15.5	2.70E-05
Unknown	3	23	3.89E-05
Total	**13**	**100**	**1.69E-04**

From the above data we can see that majority of the failures are caused due to equipment failure which can be attributed to the poor maintenance of valve or a gasket subcomponent of the pipeline. Hence, proper inspection and operation of pipelines is an important criterion to prevent these types of hazards.

The frequency of leaks due to full-bore ruptures is much less when compared to the small and medium leaks as described in Table 3. Therefore, modeling of large leaks would be only appropriate to determine the maximum consequence scenario. In the present thesis, realistic impact from a leak size of 11.94 mm is selected as per the experimental setup which has the second highest frequency of failure. The frequency distribution occurring at different engineered on-shore module systems in a standard CCS plant as per the leak size can be represented in the following table:

Table 5: Failure frequency distribution per year with respect to leak size (Vendrig, Spouge et al. 2003)

Module description	Failure Frequency per year			
	Small (3-10 mm)	**Medium (10-50 mm)**	**Large (50-150 mm)**	**Full-bore (>150 mm)**
CO_2 recovery at source	$9.6x10^{-2}$	$5.1x10^{-2}$	$2.0x10^{-3}$	$5.6x10^{-3}$
Converging pipelines	$3.5x10^{-3}$	$8.8x10^{-4}$	$1.0x10^{-4}$	$1.5x10^{-4}$
Booster station	$3.5x10^{-2}$	$3.8x10^{-3}$	$3.0x10^{-4}$	$8.8x10^{-4}$
Pipelines	$1.4x10^{-4}$	$9.5x10^{-5}$	$2.0x10^{-5}$	$8.5x10^{-5}$
Injection plant	$1.2x10^{-1}$	$5.3x10^{-2}$	$2.1x10^{-3}$	$5.8x10^{-3}$

1.8 Crack Propagation and Design Specifications

One of the major issues in the pipeline leakage scenario is the crack or fracture propagation. This should be addressed by installing crack arrestors at regular intervals. Crack arrestors are typically occasional pipeline joints with greater wall thickness than the pipe and better hoop stress properties (Global CCS Institute 2014). For a given stagnation temperature and pressure, the fracture propagation speed depends on the following parameters (Henning 2013) (DNV 2010):

- Wall-thickness of the pipe
- Material properties
- CO_2 composition (affects the phase diagram and thermodynamic properties of CO_2 when impurities are present)- presence of impurities such as H_2, N_2, CH_4 lower the critical temperature of CO_2 thereby increasing the toughness required to arrest ductile fracture
- Initial stagnation/operating pressure- higher the stagnation pressure, higher will be the decompression speed
- Initial stagnation/operating temperature- higher the temperature, higher will be the saturation pressure

A precise representation of the fracture control plan can be depicted as below:

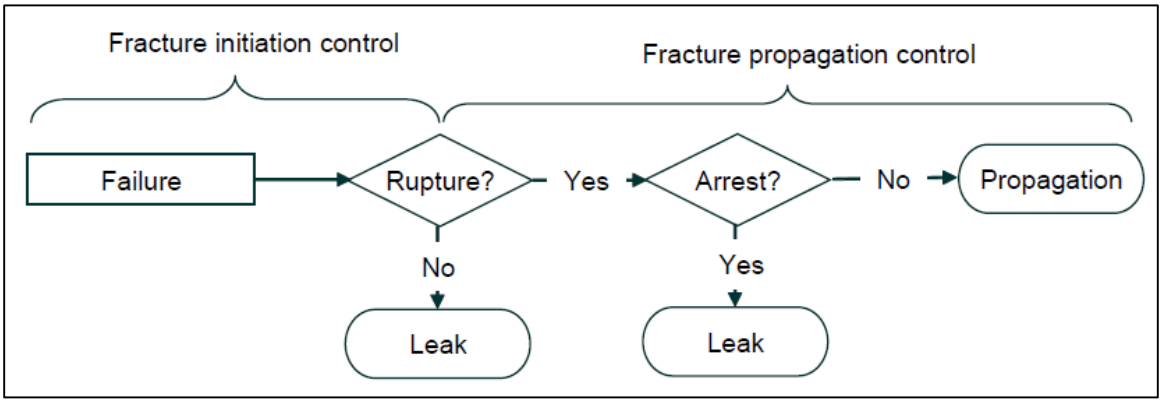

Figure 6: Fracture control plan (Cosham and Eiber 2007)

The rule of thumb for preventing ductile running fractures is (DNV 2010):

- Decompression speed of the fluid > Fracture Propagation speed
- If $P_A > P_{C,}$ then the fracture will arrest

  where P_A = Fracture arrest pressure (determined based on pipeline design parameters like pipe diameter, specifications of the material and the pipe wall thickness)

  and P_C = Critical (saturation) pressure of the CO_2 stream which depends on the CO_2 composition

For a low design pipeline having thin walls, there is a greater risk of ductile fractures as the margin between P_A and P_C would be small. Hence, choosing the right crack resistant line-pipe material forms an important criterion during construction.

For design pressures <150 bar, the risk of ductile crack propagation is more compared to higher design pressures (Henning 2013). In the present work, the design pressure considered is high enough (150 bar) for the decompression speed to be greater than the fracture propagation speed which is calculated by Mahgerefteh, Brown et al. (2012). Hence, for simplicity, it is assumed that for the given pure CO_2 (free of impurities) at supercritical conditions and for a given material of construction, there is no crack propagation. Also, after a careful assessment of the near-field

modeling results, it was observed that there was no dry ice formation observed interior of the pipe for the given leak diameters considered which would lead to interior choking and further crack propagation. This is discussed further in the following chapters.

1.9 Block Valves and Check Valves to Prevent Further Loss of Contaminants

Block valves and check valves operate like gateways for a certain section of the pipe and are usually installed to stop the flow across that section in case of a rupture. They are placed at regular intervals along the pipeline to automatically or manually receive signals in case of a pipeline failure and prevent further inventory being released into the atmosphere. While the block valves reduce the volume of the released CO_2 in case of pipeline failure, the check valves prevent the reverse flow in the pipeline.

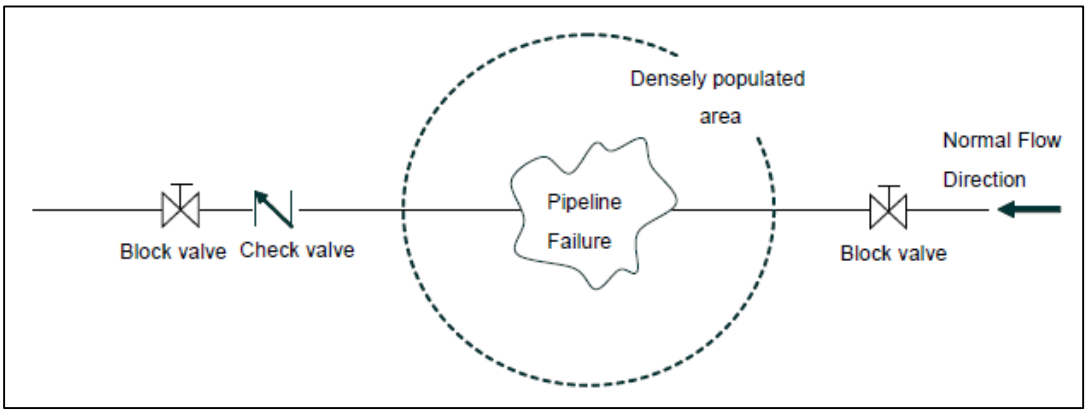

Figure 7: Placement of block valves and check valves to prevent back flow (DNV 2010)

The distance between two successive block valves has to be optimally selected due to cost implications. Too far spacing between the block valves can increase the risk of excess outflow volume of CO_2 in case of undesirable CO_2 leak and too close spacing can increase the cost of the pipeline assembly as well as enhance the risk of leakages caused due to the block valves themselves.

Therefore, depending upon the length of the pipeline between the source and the sink, the optimal number and spacing between the block valves is selected.

1.10 Planned Releases due to Failures

There could be various reasons which could obstruct the smooth transportation of CO_2 from the capture plant to storage site. Whenever there is an uncontrolled release of CO_2 either due to rupture or operational errors like tripping of an export compressor or short term planned unavailability of the reception facilities at the point of injection into storage (Dixon and Hasson 2007), the plant releases the CO_2 in a planned manner into the atmosphere in gaseous form. This allows the smooth execution of the background plant and takes into account the failure scenarios in a CCS project.

The vent is usually located at very high altitudes such as a stack at an on-shore site, or potentially on the flare tower of an offshore CO_2 injection, and operates at a variety of temperatures from close to sublimation to over 100 ^oC (Dixon and Hasson 2007). This addresses the problem of backflow or pressure build up during pipeline failures and still allowing the operation of the source from which CO_2 is captured.

1.11 Effects of CO_2 Inhalation by Humans at Various Concentrations

Depending upon the concentration and time periods of exposure to CO_2, there can be different consequences. Above certain tolerable limits, CO_2 can act as an asphyxiant and under extreme conditions of exposure can be fatal. Due to the higher density of gaseous CO_2 under normal temperature and pressure, it accumulates in low-lying populated areas and can be even dangerous. The table below presents the different acceptable levels of CO_2 and different exposure time limits. The upper limit on the acceptable amount or concentration of CO_2 inhaled in a particular location or work place is known as the occupational exposure limit (OEL). The OEL as per NIOSH 1996 (US) and OSHA (US) is 0.5% CO_2 for an exposure time of 10 hours (time weighted average). The

maximum OEL as per the Federal occupational and health regulation (US) is 4% for an exposure time of less than 1 minute.

Table 6: Consequences of exposure to CO_2 at various concentrations and time intervals (Vendrig, Spouge et al. 2003)

CO_2 concentration in air		**Exposure Time**	**Effects**
Percent (% v/v)	**ppm**		
17-30%	170,000-300,000	Within 1 minute	Loss of controlled and purposeful activity, unconsciousness, convulsions, coma, death
>10-15%	100,000-150,000	1 minute to several minutes	Dizziness, drowsiness, severe muscle twitching, unconsciousness
7-10%	70,000-100,000	Few minutes-1.5 minutes to 1 hour	Unconsciousness, near unconsciousness, Headache, increased heart rate, shortness of breath, dizziness, sweating, rapid breathing
6%	60,000	1-2 minutes-<16 minutes- Several hours	Hearing and visual disturbance, Headache, dyspnea, tremors
4-5%	40,000-50,000	Within a few minutes	Headache, dizziness, increased blood pressure, uncomfortable dyspnea
3%	30,000	1 hour	Mild headache, sweating, dyspnea at rest
2%	20,000	Several hours	Headache, dyspnea upon mild exertion

CHAPTER II

THEORITICAL FRAMEWORK AND LITERATURE REVIEW

2.1 Joule-Thomson Effect (or Joule-Thomson Expansion)

The Joule-Thomson effect essentially a temperature change that a real gas undergoes when it's pressure is changed due to sudden changes in the cross-section such as when it is forced through a nozzle or a valve. This occurs considering an isenthalpic expansion i.e. the nozzle is kept insulated and there are no heat interactions with the surroundings. The Joule Thomson equation is given as:

$$\mu_{JT} = \left(\frac{\Delta T}{\Delta P}\right)_H, \quad where \quad \mu_{JT} = \text{Joule} - \text{Thomson coefficient} \qquad (\mathbf{1})$$

A positive Joule-Thomson coefficient indicates that the gas cools when it is passes through a nozzle while a negative Joule-Thomson coefficient indicates that the gas warms or the temperature increases with decrease in the pressure. It is observed experimentally that the Joule-Thomson coefficient for CO_2 at 1 atm and 298 K is about $\boldsymbol{\mu}_{(CO2)}$=11 K/MPa (Atkins and De Paula 2006) which states that for every 1 MPa decrease in the pressure, there is a 11 K decrease in temperature. Hence for the present case where the pressure falls from 15 MPa to 0.1 MPa, the calculated value of temperature drop as per the equation (1) will be almost 164 K. This cools the fluid significantly forming dry ice below the sublimation point. In the present case, it is observed that the temperature falls to less than 173 K which is much below the freezing point of CO_2.

Hence, dry ice formation is observed during the sudden depressurization process, which is similar to flow through a nozzle explained in the later sections. This unusual phase change behavior poses a great challenge while designing the dispersion model for predicting the toxic cloud extents.

2.2 Choking Effect

As mentioned in the previous sections, favorable transportation conditions for CO_2 is usually in the dense or supercritical phase and typically in the range of 10-15 MPa pressures and 35 ^{o}C (Henning 2013). In case of a leak, when this high pressure gas comes in contact with ambient pressure, it results in a 'choked flow' at the orifice exit plane. A flow is called choked flow when the velocity of the jet attains the speed of sound in the gas as it passes through a restriction such as the throat of a converging-diverging nozzle. The mass flow rate in this type of nozzle is a function of the backpressure or the downstream pressure and it continuously increases as we reduce the downstream pressure. As we further reduce the backpressure, there is a disturbance pressure wave that is transmitted upstream which affects the flow. This pressure wave, in turn, sends a new signal downstream with enhanced flow characteristics. In the process there is point achieved where further reduction in the downstream pressure does not increase the mass flow rate further and it remains constant. At this point, the flow is said to be choked and the corresponding mass flow rate is called the 'critical mass flow rate' ($\dot{m}_{crit}$) and the corresponding downstream pressure is called the critical pressure (p_{crit}). This is illustrated in the figure below. The Mach number at this choked point condition is Ma=1 (sonic condition)

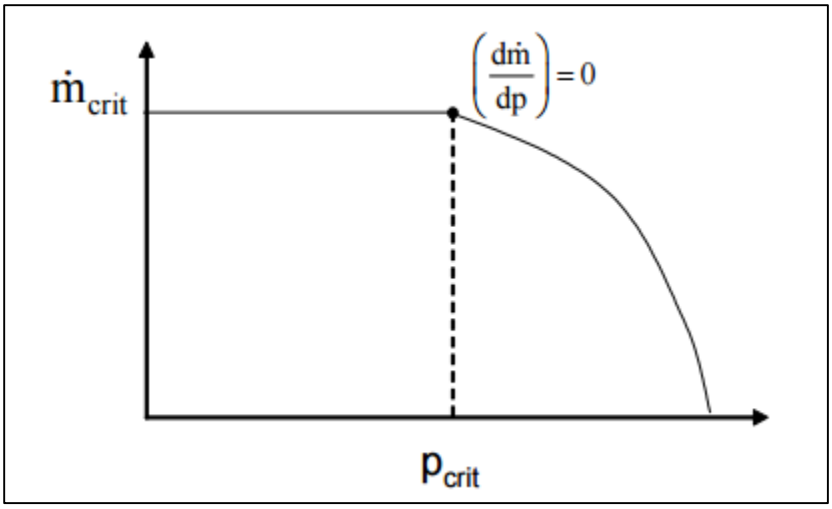

Figure 8: Variation of mass flow rate with downstream pressure (VDI-WA 1997)

In the case of a leak from a pipeline the downstream pressure is ambient pressure and it is observed that for the given supercritical upstream pressure conditions, the flow is choked at the nozzle exit.

At the nozzle exit, the pressure is still above the ambient pressure ($P_{exit}>P_{amb}$) and this leads the jet to expand beyond this point and is called an 'under expanded jet' (Cumber, Fairweather et al. November 1995). The jet expands enough such that the pressure after certain distance reaches below the ambient pressure (back pressure) and the jet reflects in the form of an oblique shock. Hence, the expansion of this under expanded jet is accompanied by the formation of series of expansion and compression shock waves that propagate along the jet flow. This expansion and compression pressure waves form a unique pattern which are in the form of shock diamonds and hence called as 'Mach disks' or 'Mach diamonds' as shown in figure 9. For an ideal gas, the pattern continues infinitely while for a viscous real gas case, the jet undergoes turbulent mixing with the surrounding atmosphere and gradually decays after a certain distance with a small number of cycles.

Usually, the rule of thumb for choked flow conditions is when the ratio of the upstream pressure to the ambient pressure exceeds $\left[\left(\frac{\gamma+1}{2}\right)^{\frac{\gamma}{\gamma-1}}\right]$ where the heat capacity ratio, $\gamma = C_p/C_v$. For CO_2, this ratio of upstream to ambient pressure is 1.83 and hence, the flow is said to be choked. The series of Mach discs or shocks created due to this choked flow are discussed in the results section. The typical mass flow rate when the flow is choked can be calculated using the formula below [10]:

$$\dot{m} = C\,A\left(\gamma\,\rho\,P\left(\frac{2}{\gamma+1}\right)^{\frac{\gamma+1}{\gamma-1}}\right)^{0.5} \qquad (\mathbf{2})$$

where, $\dot{m}$ = mass flow rate (kg/s)

C= Coefficient of discharge (usually taken as 0.72)

A= cross-sectional area (m^2)

γ = ratio of specific heats= C_p/C_v (usually 1.29 for CO_2)

ρ = density of the fluid at supercritical temperature and pressure (kg/m^3)

P= Absolute stagnation pressure (Pa)

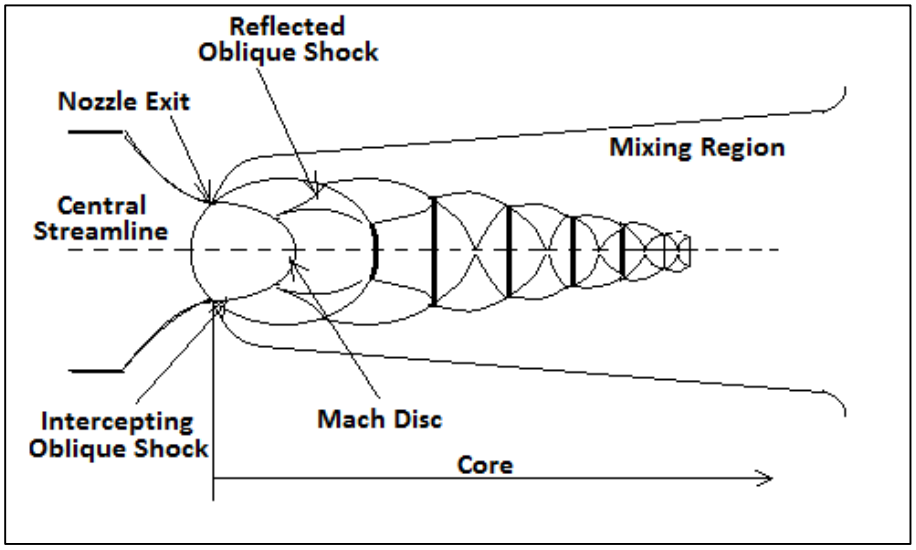

Figure 9: Series of shock waves (Mach disks) (Kaushik, Kumar et al. 2015)

In the present case, the release was considered to be horizontal, or parallel to the direction of wind. Such cases are mostly observed where leak is generally located near a pipe bend or in the vicinity of a flange. The pipeline orientation for a leak in the area of the bend is illustrated in the figure below.

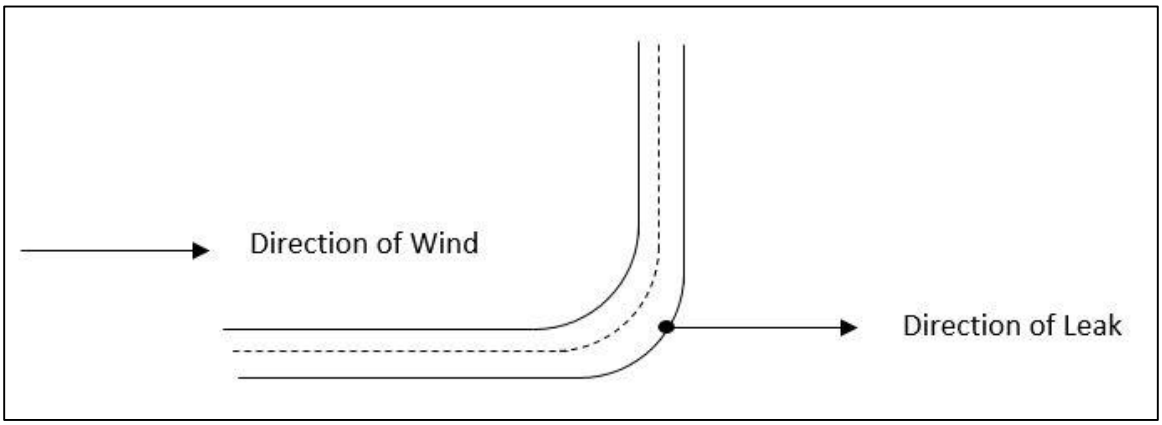

Figure 10: Horizontal leak illustration

2.3 Motivation

Effective management of CO_2, among all other greenhouse gases, is one of the major challenges that we are facing today to reduce the impact of global warming. The decrease in the anthropogenic emissions by effective management of CO_2 could bring down the atmospheric CO_2 levels to about 33% (Sun, Wang et al. 2002). One of the efficient ways to combat climate change is to capture this CO_2 emitted from anthropogenic sources and store them. Carbon Capture, transport and storage (CCTS), as discussed above, is a very effective technology which involves a series of steps from carbon capture and sequestration until storage. Pressurized pipelines are considered to be one of the most efficient ways for transporting large volumes of CO_2 especially when the storage site is located at long distances from the emission source. Safe transportation of CO_2 through long distance pipelines in either dense phase or supercritical phase is thus one of the most sought after fields of investigation. A lot of expertise has been developed in the last few years

over the transportation of natural gas and methane, but cost-effective technologies developed for the long distance transportation of CO_2 is scarce (Woolley, Fairweather et al. 2013). Due to the unique thermodynamic properties of CO_2, there is a limited knowledge about the after physics in case of a leakage of pipeline and this poses a greater challenge in terms of correctly predicting the eventual concentrations of CO_2 during dispersion modeling. Handling supercritical releases in an unlikely event of depressurization can be complex as CO_2 directly undergoes transition from dense phase liquid to a two-phase gas/solid mixture which can be challenging to model. Unlike modeling of natural gas which involves handling only two-phase (liquid and gas) post-leakage, CO_2 modeling involves handling all three phases (solid, liquid and gas) at the same time immediately close to the leak exit in near-field dispersion.

Gaseous CO_2 at atmospheric conditions possesses a density of 1.98 kg/m^3 which is 1.5 times that of air. Hence, whenever there is a leakage from an above-ground pipeline infrastructure, there is an increased risk of accumulation in case of obstacles, such as buildings, in low-lying areas. There a greater need to quantify and model the safety and environmental aspects of CO_2 pipeline transportation over long distances which often pass through populated areas. CO_2 is an asphyxiant and toxic above 5% concentrations and potentially fatal above concentrations of 10% (NIOSH 1996).

In order to develop cost-effective solutions for the dense and supercritical transportation of CO_2 through pipelines, a detailed and accurate modeling of the leak phenomena is required. The most conservative approach as per Hanna, Drivas et al. (1996) is to assume the release direction to be horizontal. Accurate source term modeling and its subsequent dispersion modeling forms the base for accurately predicting and preventing the harmful release of CO_2 in air. This data can, in turn, serve as a risk basis tool for pipeline design and for planning emergency evacuation in case of an accidental release.

This paper is divided into two parts- the first part deals with the near-field dispersion modeling in which the release rate of the CO_2 post leakage is calculated by taking into consideration

the accurate thermodynamic models for density and the physical state of the escaping CO_2 is determined based on CFD results. The pseudo-source properties are taken from the model-1 and is used as an inlet for model-2 which deals with the far-field dispersion modeling of CO_2. This paper deals with CO_2 pipeline maintained at supercritical conditions of 15 MPa and 420 K which are validated in accordance with experiment 8 (horizontal release) carried out for BP DF1 CO_2 at Spadeadam site (UK) (Witlox, Harper et al. 2014).

2.4 Source Term Modeling

The rupture in the CO_2 pipeline is accompanied by generation of an under-expanded jet from the point of leak that has a high velocity and momentum. It contains gaseous CO_2 along with fine dispersed solid CO_2 particles also known as dry ice. The evaluation of the source terms means evaluating the properties of this initial jet from the point of release until it reaches the atmospheric pressure. In order to determine the source strength of this time varying jet, we need to determine factors such as the velocity, density, temperature, pressure and vapor mass fraction. This in turn is useful in determining the mass flow rate or the release rate of the jet.

The hazard analysis for determination of the final concentration after leak cannot be done in a single step as the near-field release scenarios cannot be captured clearly and is computationally inefficient. In addition, the measured time and length scales of the expanding waves in the near-field dispersion modeling are very small when compared to the far-field model. The process of predicting the behavior and final concentrations of CO_2 in a single step takes significantly long computational times with minimum outcome. Hence, the risk analysis of the accidental leakage scenarios is done in two steps: the first step involves determining the source strength or the pseudo-source characteristics; and the second step involves using the source term values to predict the far-field concentrations in the dispersion modeling.

The first step towards risk analysis is the near-field modeling or the source term modeling. Source strength or the release rate of the high speed jet is usually determined at a distance

downstream of the leak which serves as an input in the later dispersion modeling. Hence, accurate source-term modeling becomes the primary criteria for correctly determining the concentrations of accidental supercritical CO_2 releases in further dispersion modeling.

A number of theories were formulated to calculate the effective release rate at the exit plane. The earliest among them was suggested by (Dixon and Hasson 2007) where sonic and choked flow condition were assumed at the exit plane. Release rate was calculated for non-flashing liquid releases by taking help of the Venturi effect and Bernoulli's principle was applied. The mass flow rate in this case would be given by $\sqrt{2\rho\Delta p}$ and the value of Δp is given by $(p_S - p_a)$ where p_S is the stagnation pressure and p_a is the atmospheric pressure. This approach is however valid only for non-flashing liquids since flashing liquids do not necessarily have atmospheric pressures at the exit planes. This method is also found to be applicable to gaseous releases (Dixon and Hasson 2007). Usually a sonic release is assumed at the exit plane for a pure gaseous release (Global CCS Institute 2014).

For dense phase or liquid phase releases, the jet flashes at the exit plane and changes to solid and vapor phase. A more appropriate way to deal with flashing liquid releases from inventory is to assume temperature to be constant for a sub-cooled liquid. This is true because the constant temperature and entropy lines are found to be parallel in the p-h diagram which implies that the pressure at the exit plane would be the saturation pressure at the given temperature. A more exact method applied was the Homogenous Equilibrium Model (HEM) which assumed that mechanical and thermodynamic equilibrium existed between the liquid and the vapor phase. This implied that they shared the same velocity and temperature and there was no slip assumed between the two phases. In addition, since both the vapor and the condensed phase are assumed to be always in equilibrium, the point always lies on the saturation line. Mazzoldi, Hill et al. (2008) calculated the release jet speed with the same assumption of choked flow rate for a high pressure leaking facility.

The Bernoulli's principle was applied to calculate the mass flow rate through an orifice under choked conditions by using the following equations:

$$\frac{v_i^2}{2} + gh + \frac{P_i}{\rho} = \frac{v_f^2}{2} + gh + \frac{P_f}{\rho} \qquad (\mathbf{3})$$

Which gives

$$(P_i - P_f) = \rho/2\ (v_f^2 - v_i^2) \qquad (\mathbf{4})$$

And as discussed in Eq. (2) for a choked flow, the choked mass flow rate can be given as:

$$\dot{m} = C\ A \sqrt{\left(\gamma\ \rho\ P \left(\frac{2}{\gamma + 1}\right)^{\frac{\gamma+1}{\gamma-1}}\right)}$$

where P_i = initial stagnation pressure inside the pipeline (MPa)

P_f = atmospheric pressure (MPa)

v_i = initial velocity inside the pipeline (m/s)

v_f = final velocity outside the pipeline soon after release (m/s)

The above set of equations do not take into consideration the leak size or the orifice diameter and hence, are same for full bore or small leak. This takes into consideration that the release rates in case of a full-bore rupture does not develop very high release speeds due to fast depressurization of the inventory.

Hill, Fackrell et al. (2011) considered isentropic expansion of the fluid from the container to the exit plane. Usually an isentropic assumption considers negligible forces acting on the free expansion surface and ambient air entrainment. The enthalpy balance equation would result in:

$$h_0 = h_e + \frac{u_e^2}{2} \qquad (\mathbf{5})$$

where h_0 = stagnation enthalpy

h_e = enthalpy at the exit plane

u_e = velocity at the exit plane

The mass flow rate per unit area (G) at the exit plane would then result in:

$$G = \rho_e u_e = \sqrt{2\rho_e^2(h_0 - h_e)} \qquad (\mathbf{6})$$

Hill, Fackrell et al. (2011) also considered homogenous equilibrium conditions for the two phase flow between the orifice exit until the jet reaches ambient conditions. Conservation laws are applied in this expansion region. The source term parameters were based on these assumptions and maximum mass flux was set at the saturation release conditions. This fixes the sublimation temperature of -78.5 ^{o}C on the PV curve at a constant ambient pressure of 1 atm.

The main forces that effect the discharge rate of a fluid are the pressure gradient and the gravitational forces. Until the inventory is fully depressurized to ambient conditions, the pressure forces govern the discharge rate. After this point, the gravitational forces take hold and depend upon the angle of inclination of the pipeline.

At any given point on the axis of the nozzle, the source strength is observed to gradually decrease with time. This is because there is a decrease in the mass flow rate over the period of time as the inventory is exhausted. A single time-averaged value of the release rate is calculated from the first model which serves as the input boundary condition in the second model. This method is usually found to be reasonable as the depressurization takes place rapidly.

2.5 Thermodynamic Equation of State

Selecting the right real gas Equation of State (EOS) is very important as this can accurately predict the thermodynamic properties of the mixture over a wide range of temperatures and pressures. It is observed that even slight variations in density inputs can widely vary the source characteristics in the model. Liu, Godbole et al. (2014) and Zalosh and Hung (1994) used ideal gas law to compare the value of the CO_2 release rates as well as downstream CO_2 concentrations with the experimental values. It is inappropriate to consider ideal gas in cases which involves pressures close to critical point or higher. It usually serves as a better approximation when the pressures are very low of the order of atmospheric pressures. Further, important source terms like density are

under-predicted by ideal gas assumption. Peng-Robinson can very well predict the mass density of the supercritical CO_2 at the given conditions (Mazzoldi, Picard et al. 2013). Hence, Peng-Robinson equation of state was chosen as the method for predicting the properties of CO_2.

The source term in the present case was determined in Ansys Fluent V16.2.

The pressure for a Peng-Robinson equation of state can be given as:

$$P = \frac{RT}{v-b} - \frac{\delta a(T)}{v(v+b)+b(v-b)} \qquad (7)$$

where T = temperature (K)

v = molar volume (cu.cm/mol)

R = universal gas constant (cu.cm MPa/K mol)

The values of constants 'a', 'b' and $'\delta'$ are given by:

$$a = 0.45724\ (RT_C)^2/P_C$$

$$b = 0.0778\ (RT_C)/P_C$$

$$\delta = \left(1 + k\left(1 - \sqrt{T_r}\right)\right)^2$$

$$k = 0.37464 + 1.54226\omega - 0.26992\omega^2$$

ω = accentric factor

T_r = reduced temperature = T/T_C

T_C = critical temperature (K)

Woolley, Fairweather et al. (2013) and Mazzoldi, Picard et al. (2013) had accounted for the composite equation of state for calculating the gas-solid phase properties. They included Peng-Robinson equation of state for gas phase property calculation and Span and Wagner (1996) equation of state for condensed phase (solids) to take into consideration the discontinuities of properties at and below the triple point of CO_2. Although the Peng-Robinson equation shows discontinuities in the presence of solid phase and vapor phase mass fraction below the triple point when compared to the pure CO_2 equation of state, there is no significant difference in the prediction

of the critical mass flux between the two methods. Hence, Peng-Robinson equation of state was found to be reliable for predicting the mass flow rate of the depressurization process (Mazzoldi, Picard et al. 2013).

2.6 Physicochemical Characteristics of Expanding Jet

At the start of a blowdown, the initial pressure of single phase supercritical fluid in the pipeline falls to the saturation pressure. A dense phase is formed at this point which boils giving rise to vapor dome on the liquid layer. This liquid layer gradually decreases as the fluid approaches the exit plane and produces vapor CO_2 with entrained liquid droplets. At this plane, the flow is observed to be choked for the given stagnation conditions. Beyond the nozzle exit plane, flashing occurs and there is a sudden decrease in temperature due to Joule Thomson effect which converts the entrained liquid droplets into solid once the temperature falls below the triple point of CO_2. Therefore, the fluid is generally a mixture of all three phases i.e. solid/gas, liquid/solid and gas/liquid after this point (Innovation June 2015).

The resulting jet expands in a 'tulip' shaped fashion due to a series of shock waves and can be divided into two zones as shown in figure 11. The zone immediately next to the exit plane (p_b) till the mixture reaches atmospheric pressure (p_a) is marked as the 'depressurization zone' in which all liquid is flashed into vapor and the air entrainment is minimal. It is assumed that mass, momentum and energy are conserved in the depressurization region. In the present case, it is observed that the end of depressurization zone is approximately 3.5 times the diameter of the orifice away from the exit plane where the pressure reaches atmospheric pressure condition. The heat required in this region for liquid evaporation is taken at the expense of the vapor cloud and this further reduces the temperature resulting in solid particles. Dixon and Hasson (2007) poorly predicted the solid CO_2 particle concentration in their model by adding scalar quantities via source

terms to the transport equations. The assumption of constant particle diameter was made while calculating the heat and mass transfer between the solid particles and the surrounding gas phase.

The depressurization zone further expands into an 'entrainment zone' or the two-phase zone which essentially contains only solid and gas phases (as CO_2 triple point is above 1 atm). The velocity of the jet slowly decreases as it moves from the leak. As the name suggests, in the entrainment zone, the rate of air entrainment increases beyond point 'a' and we can observe that there is mixing between the jet and the ambient air. Since the entrainment zone involves a wide range of temperature change (ranging from -78 ^oC to atmospheric temperature), the moisture in the surrounding air is condensed into water droplets which makes the colorless expanding CO_2 gas dispersion visible to the naked eye. This will be evident until the temperature of the cloud increases above the dew point of air. Witlox, Stene et al. (2011) studies have concluded that the presence of water vapor in the dispersing plume has limited effect on concentration measurements in the far-field.

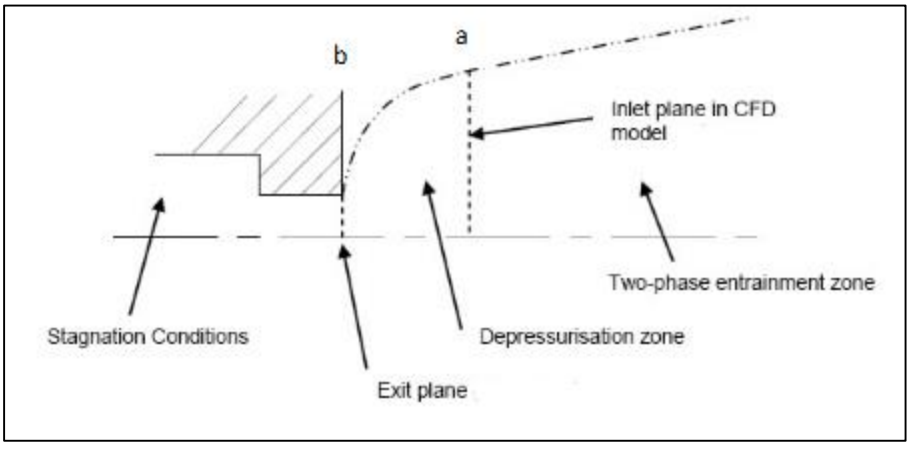

Figure 11: Division of zones of the jet (Dixon and Hasson 2007). Here pressure at the inlet plane is ambient pressure.

It is usually difficult to carry out the dispersion modeling with the existing complex conditions at the nozzle exit. Hence, a 'pseudo source' which is the end of the depressurization zone at atmospheric pressure (point a) is fixed and the source term conditions like temperature (T_a),

velocity (v_a), jet area (A) and vapor mass fraction (x_v) are calculated. These conditions are taken as input conditions for the dispersion model. In order to design the entire phenomena of decompression and ambient air mixing, the near-field model takes into account the phase changes occurring close to the leak and fixes the pseudo source point which in turn determines the input mass flow rate, temperature and mass fraction of CO_2 that have to be input as boundary conditions into the far-field dispersion model.

Most of the mathematical methods that consider theoretical calculation of the pseudo source conditions make certain assumptions over the depressurization zone. The only drawback by doing so is that you can calculate properties like temperature, density and velocity of the jet after expansion but this method cannot predict the distance from the nozzle exit to the pseudo source. Hence, these are zero-dimensional methods. A CFD model is a robust model which can accurately predict the pseudo source terms conditions as well as correctly determine the effective length from the nozzle exit that can be used in the dispersion model. Usually, the point 'a' is not far away from the nozzle exit. In the present case, the pressure quickly falls to the ambient pressure at a distance of 0.04107 m from the nozzle.

As we move further downstream in the expansion zone, the jet starts to lose momentum and the gas dispersion in this region is solely governed by the turbulence which affects the air and gas mixing effects. Depending upon the upstream pressure conditions and the length and diameter of the inventory, the release will continue and the cloud will keep growing in size until all the inventory is expended. Downwind, the cloud will entrain air and depending upon the turbulence model will determine to what extent the cloud will disperse. Hence, choosing the right turbulence model is important governing factor which determines downwind dispersion.

The mathematical simulation of the dispersion of CO_2 in air is solved by Fluent by using CFD tools such as Navier-Stokes equations. The transport equations are then closed by using different turbulence models such as k-ε, k-omega or k-l.

Reynolds averaging is usually performed for transient simulations to study the effects of turbulence by Reynolds or time decompositions. Hence, this method is termed as Reynolds (or time) averaged Navier-Stokes (RANS). The variables fluctuating due to turbulence can be decomposed or broken down into a mean part and a fluctuating part.

$$\phi(t) = \bar{\phi} + \phi'(t) \quad (\mathbf{8})$$

where $\phi(t) =$ fluctuating turbulent variable in RANS

$\bar{\phi} =$ Mean part

$\phi'(t) =$ fluctuating part

The mean part can be obtained by time-averaging the variables as:

$$\bar{\phi} = \frac{1}{\tau}\int_0^{\tau} \phi(t)\, dt \quad (\mathbf{9})$$

where $\tau = large\ time\ period$

The governing equations for RANS in Cartesian coordinates can be written as:

Mass Continuity:

$$\frac{\partial \rho}{\partial t} + \frac{\partial}{\partial x_i}(\rho u_i) = 0 \quad (\mathbf{10})$$

Momentum Equation:

$$\rho\frac{\partial}{\partial t}(u_i) + \rho\frac{\partial}{\partial x_j}\left(u_j u_i + \overline{u_i' u_j'}\right) = -\frac{\partial P}{\partial x_i} + \frac{\partial}{\partial x_j}\left(\mu\frac{\partial u_i}{\partial x_j}\right) + \rho\mathbf{g} \quad (\mathbf{11})$$

Equation for mass fraction:

$$\rho\frac{\partial}{\partial t}(\beta) + \rho\frac{\partial}{\partial x_j}(u_j\beta) = \frac{\partial}{\partial x_j}\left[\left(\frac{\nu_t}{Sc_t}\right)\frac{\partial \beta}{\partial x_j}\right] \quad (\mathbf{12})$$

Here solid phase fraction is negligible since they sublimate quickly within the plume and hence the solid gas dispersion is assumed to obey the same conservation equations of flow as that of the gas phase. This implies that the turbulent fluctuations are same for both solid and vapor CO_2 in dispersion modeling.

where ρ = density of fluid (kg/cu.m)

t = time (s)

u_i *and* u_j = velocity in the i and j direction (m/s)

x_i *and* x_j = components of the coordinate vector x (m)

u_i' *and* u_j' = fluctuating velocities (m/s)

$\overline{u_i' u_j'}$ = Reynolds stress tensor (R_{ij})

P = Pressure (Pa)

g = acceleration due to gravity (m/s^2)

β = vapor mass fraction of CO_2 vapor

ν_t = kinematic turbulent viscosity (m^2/s)

Sc_t = Schmidt number = constant = 1.0 (Alinot and Masson 2005)

The unknowns in the RANS are the turbulent stresses $\left(\overline{u_i' u_j'}\right)$ which are solved by using the two-equation standard k-ε turbulence model which are described in the later sections. These differential equations for mass, momentum and energy are solved in a finite-volume approach by using an unstructured mesh on distinct control volumes in a 3D space. An implicit pressure based solver solves the coupled set of pressure-velocity equations. The spatial discretization is achieved by using second order upwind schemes for pressure and momentum.

2.7 Pasquill Atmospheric Stability Class

Determining the stability class is important to determine the amount of turbulence at any given time of the day. As the degree of turbulence increases, the pollutant concentration dispersion in air increases thereby increasing the air entrainment. Dispersion is the spreading of pollutant from a high concentration to a low concentration. The classification of the stability classes depends on whether the given air mass or packet is either rising in air or tending to stay in the same position or sinking depending upon the rate of change of temperature in the atmosphere. If the given air mass

tends to rise due to its buoyancy, it is considered as an unstable condition whereas if it tends to stay in the same position or sink, it is said to be a stable condition. This temperature flux arises due to the sun's radiation during the day which causes the high degree of mixing (turbulence) between the consecutive fluid layers which leads to instability.

Depending upon the atmospheric turbulence, there are six stability classes defined by Pasquill (1961). They are listed in the table 7, below:

Table 7: Pasquill stability classes (Pasquill 1961)

Stability Class	Stability criteria
A	Extremely unstable
B	Moderately unstable
C	Slightly unstable
D	Neutral
E	Slightly stable
F	Moderately stable

During the day, due to solar radiation, the air close to the ground tends to warm up and rise causing instability. From the table above we can see that the classes A, B and C are unstable which means that these classes occur during the day when there is maximum mixing in air. Class D occurs either when there is an overcast during a day or at night. Classes E and F occur during the night when the cool dense air is near the earth's surface and low wind speeds due to no mixing. These classes affect both the horizontal and vertical mixing of the plume. This can be depicted clearly in the following table:

Table 8: Wind speed correlation to stability classes (Woodward 2010)

Wind Speed (m/s)	DAY TIME Incoming solar radiation			NIGHT TIME Cloud cover	
	Strong	Moderate	Slight	Thin overcast or >1/2 low clouds	<3/8 cloudiness
<2	A	A-B	B	-	-
2-3	A-B	B	C	E	F
3-5	B	B-C	C	D	E
5-6	C	C-D	D	D	D
>6	C	D	D	D	D

In the present thesis, the experimentally recorded conditions align with either overcast or high wind speeds. Also, thermal radiation values in the experiment from the sky and ground are minimum and hence neutral stability class conditions (D) is considered. This can also be verified from the velocity measurements in experiment 8 which is 5.5 m/s-6.1 m/s.

2.8 Turbulence Modeling

2.8.1 Atmospheric Boundary Layer (ABL)

The atmospheric boundary layer is the region in the atmosphere where the majority of the exchange of momentum, heat and pollutants transfer takes place. This region might extend from a few meters to several kilometers from the earth's surface depending upon these parameter interactions. This is an important factor for determining the size of the largest eddies or indirectly, the time and length scales of a particular parameter, which directly influence the turbulence in the numerical simulations in dispersion modeling. While dealing with turbulent flows, we need to determine the size of the largest eddy we are dealing with, which is typically called as the length scale and the subsequent smaller eddies are determined based on this length scale. The time scale is the length of the largest eddy by the flow. This is also addressed as 'large eddy turnover' and is

given as L/U. It is observed that an atmospheric boundary layer time scale is typically 1 hour meaning the surface forcings are captured from the earth's surface to a vertical height up to 1 hour.

The Atmospheric Boundary layer can be divided into a number of sub-layers: the layer which is closest to the ground, the surface layer and the Ekman layer. As we increase in height, the shear-stress component decreases. We need to have a law which can give us a relationship between the mean wind velocities with respect to the vertical wind velocity at a reference height. Under fully-developed conditions, we can define the vertical component of velocity by an empirical power law correlation which can be written as:

$$\frac{\bar{U}(z)}{U(H)} = \left(\frac{z}{H}\right)^{\alpha} \qquad (\mathbf{13})$$

where $\bar{U}(z) =$ mean wind velocity at a vertical point z from the ground (m/s)

$U(H) =$ mean vertical wind velocity at reference height H from ground (m/s)

$z =$ roughness height at which the wind velocity is being computed (m)

$H =$ reference height (m)

$\alpha =$ shear-stress exponent = (1/7) for neutral conditions and flat terrain

$'\alpha'$ is generally a function of the height in consideration and the surface roughness (z_0).

On the contrary, Mazzoldi, Picard et al. (2013) considered logarithmic wind profiles in the surface layer to calculate the ambient mean wind speeds over the domain. The mean horizontal velocity in case of a log wind profile is given by:

$$\frac{\bar{U}(z)}{u_r} = \frac{1}{\kappa}\left(\frac{z}{z_0}\right) \qquad (\mathbf{14})$$

where $u_r =$ mean reference wind speed (m/s)

$z_0 =$ reference height (m)

$\kappa =$ von Karman constant

The wind power law is generally a good approximation of the log wind profile by taking into account all aspects of surface roughness and atmospheric stability through the shear exponent.

The value of shear exponent is reported as 1/7 for neutral stability conditions for heights under 50 m (Peterson and Hennessey 1978). This relationship is usually helpful when the surface roughness or atmospheric stability condition is not available readily. This law generally holds good for assessing the desired value of wind conditions at a certain height by adjusting it to standard height wind velocity conditions.

In the present thesis, the concentrations are tested at various locations from the source by taking into consideration both the mean wind flow by power law as well as under constant wind flow conditions.

Once the jet reaches atmospheric pressure, there is no pressure gradient to induce fluid motion, and hence after this point, the gas dispersion is only a factor of the turbulence model which further determines the air and CO_2 mixing. This in turn determines the amount of air entrainment in the dispersing jet which leads to the dilution of dispersing CO_2. Hence, choosing the right turbulence model is an important criterion in CO_2 gas dispersion.

2.8.2 Standard k-ε Turbulence Model

Standard k-ε turbulence model is a two equation model which employs two additional transport equations for turbulent kinetic energy (k) and turbulent dissipation rate (ε) to the present set of equations defined in section 2.6. The kinetic energy determines the velocity of these eddies while the dissipation rate determines the rate at which the turbulent kinetic energy is getting destroyed. They are usually adopted to close the system of partial differential equations by relating the unknown fluctuations in the RANS to the mean flow. These fluctuating terms known as the Reynolds turbulent stresses (τ_{ij}) were first related to the eddy viscosity (ν_t) by Boussinesq by the following equation:

$$\tau_{ij} = -\overline{u_i' u_j'} = \nu_t \left[\frac{\partial \mathrm{u}_i}{\partial \mathrm{x}_j} + \frac{\partial \mathrm{u}_j}{\partial \mathrm{x}_i}\right] - \frac{2}{3} k \delta_{ij} \qquad (\mathbf{15})$$

here k=turbulent kinetic energy (m^2/s^2)

and δ_{ij}=Kronecker delta (=0 if i≠j and =1 if i=j)

The eddy viscosity in the equation above can be written as:

$$\nu_t = \frac{C_\mu k^2}{\varepsilon} \tag{16}$$

The transport equations for k and ε are given below:

$$\frac{\partial \mathrm{k}}{\partial \mathrm{t}} + \mathrm{u}_j \frac{\partial \mathrm{k}}{\partial \mathrm{x}_j} = \frac{\partial}{\partial \mathrm{x}_j}\left[\left(\frac{\nu_t}{\sigma_k}\right)\frac{\partial \mathrm{k}}{\partial \mathrm{x}_j}\right] + \tau_{ij}\frac{\partial \mathrm{u}_i}{\partial \mathrm{x}_j} - \varepsilon \tag{17}$$

$$\frac{\partial \varepsilon}{\partial \mathrm{t}} + \mathrm{u}_j \frac{\partial \varepsilon}{\partial \mathrm{x}_j} = \frac{\partial}{\partial \mathrm{x}_j}\left[\left(\frac{\nu_t}{\sigma_\varepsilon}\right)\frac{\partial \varepsilon}{\partial \mathrm{x}_j}\right] + C_{1\varepsilon}\frac{\varepsilon}{k}\tau_{ij}\frac{\partial \mathrm{u}_i}{\partial \mathrm{x}_j} - C_{2\varepsilon}\frac{\varepsilon^2}{k} \tag{18}$$

where $\sigma_k \; and \; \sigma_\varepsilon = thermal \; diffusivities \; of \; k \; and \; \varepsilon$

and $C_\mu, C_{1\varepsilon}, C_{2\varepsilon} = constants$

There are a couple of constants in the above set of closure equations and their values are given in the following table:

Table 9: Values of constants for set of closure equations to RANS

σ_k	σ_ε	$C_{1\varepsilon}$	$C_{2\varepsilon}$	C_μ
1.0	1.3	1.44	1.92	0.09

Therefore, in order to evaluate the Reynolds stresses, we need the value of ν_t which is dependent on both k and ε. We can also see from equations 12 and 13 that both k and ε are interdependent on each other. Hence, all the equations are strongly coupled and have to be solved implicitly by using an appropriate solver in Fluent.

2.9 Dry-Ice Formation

As discussed above, the sudden adiabatic expansion of the gas from supercritical to atmospheric pressures can introduce the possibility of fractures in pipelines apart from the possibility of dry-ice or solid CO_2 formation. These solid particle sizes vary depending upon the

leakage orifice diameter and can go from a few μm to 0.1 mm (100 μm) Liu, Calvert et al. (2012) studied the particle size distributions along the jet flow through an expansion nozzles at different orifice diameters into a small expansion chamber of varying diameters (2, 4 and 6 mm). The three factors that affect the formation of dry ice were precisely temperature, pressure and the magnitude of the diverging section or the expansion chamber. The dry ice formation followed a consecutive process of particle deposition and re-entrainment due to sublimation inside the diverging section. Initially the smaller particles of dry ice were agglomerated on the wall due to adhesion between the particles and then depending upon the velocity of the jet, they were re-entrained into the jet. Higher orifice diameters would infer higher velocity and jet mass flow rate. As the mass flow rate increases, the agglomerates would be forced to detach from the deposition layer causing it to re-entrain into the jet. Also, as the orifice diameter increases (eg: full bore ruptures), the particle diameter increases, thereby leading to sublimation at greater distances from the nozzle outlet. The high mass flow rate resulting from such a release would take longer times to exchange heat with the surrounding atmosphere, thereby leading to late sublimation as compared to the nozzle with smaller diameters.

From the studies carried out by Rusli, Chang et al. (2014), for a supercritical storage condition of 150 bar, the particle size for a big leakage diameter of around 20 mm would cause a solid particle size of 0.94 μm which was not significant to cause a rainout. These conditions coincide with the BP's DF1 CO_2 experiment in consideration, where the stagnation pressure is 150 bar and therefore the initial dry ice particles are expected to be a very fine mist of CO_2. In addition, since the boiling point of CO_2 is -78.4 ^{0}C, the solid particles sublime very quickly within the jet. This result also coincided with the presumption of Mazzoldi, Hill et al. (2008) wherein it was concluded that for horizontal releases, there was no rainout of dry-ice. Most of the dry-ice that was formed gets sublimated within the jet due to the high mass flow rate of the supercritical release. This can be observed from the jet flow studies carried out in the present study which concludes that

the solid formation was only distributed up to few millimeters after the nozzle exit and all the solid particles were sublimated within the jet causing no pool formation or rainout.

Lankadasu, Tripathi et al. (2015) considered the solid particle modeling of the jet by adding a transport scalar to the enthalpy equation in the form of source terms to calculate the solid mass fraction. Dixon, Gant et al. (2012) followed the same method to predict the solids concentration. Since homogeneous equilibrium model was applied, 'boiling' assumption was made and the sublimation temperature was fixed to 194 K at the pseudo source point. A constant solid particle size was assumed in the depressurization region. In reality, the dry-ice particles constantly undergo sublimation in the jet, shrinking in size and turning into CO_2 vapor. But these assumptions are made for simplicity and reduced computational efforts.

Dixon, Gant et al. (2012) followed a Lagrangian particle tracking model to model the solid CO_2 particles in ANSYS CFX using a standard droplet evaporation model. Majority of the models which consider solid particles assume the solid phase is a kind of liquid phase with thermodynamic properties of solid below the triple point. This majorly simplifies the simulation of solid dry-ice particles in the sublimation process to an evaporating liquid pool model which can be viewed as liquid evaporating to form vapor.

Hill, Fackrell et al. (2011) studied the effect of presence of solids of different sizes in the released CO_2 jet. The study considers liquid evaporation model for CFD analysis in Ansys CFX. Lagrangian particle tracking method was applied to calculate the steady state release rates at the orifice measuring 0.5 m in diameter which can be viewed as a significantly large leak. The pipeline was located 5 m above ground level. Four simulations of solids ranging between 10 and 50 μm, 50 and 100 μm, 50 and 150 μm and no solids were carried out. Although the presence of solids post nozzle exit can considerably cool the CO_2 plume which stays for longer periods than vapor only releases, the results predicted that the final downwind concentrations of the plume were relatively insensitive to the CO_2 particle size. Experimental validation was not presented in this study.

Thus, the solid/vapor mixing of CO_2 with air after decompression assumes a homogeneous equilibrium without the solid deposition. In the present study, the trajectories of solid CO_2 are not modeled.

CHAPTER III

COMPUTATIONAL SETUP AND METHODOLOGY

The computational setup was done in two parts. The first part was to calculate the source strength of the jet or the jet model. This takes into consideration the transition flow and phase change of supercritical CO_2 from very high pressure pipe upon decompression. The second part accounts for the large scale dispersion of the pollutant in ambient air and calculates the concentrations in the far-field.

3.1 Experimental Setup

There were limited number of experiments conducted till date that are useful to validate the far-field dispersion models. To bridge the gaps in the understanding of transportation of large volumes of CO_2 as a part of CCS projects, BP conducted tests at Spadeadam test site in 2006, North of England. As a part of their research endeavor, the project was carried out to identify the critical knowledge gaps and address the key issues underlying the release of dense and supercritical CO_2 from pipelines. The Spadeadam site was originally operated by a global engineering company 'Advantica'. One of the aspects was to provide modelers necessary validation data for predicting the outflow and dispersion models from these high pressure releases. The results were finally made available to public by Det Norske Veritas (DNV) in May 2012.

A total of 12 experiments were conducted by BP in both liquid and supercritical (dense) phases, all of which were horizontal releases. Out of these 12 experiments, Trial 8 and 8R (Repeat of Experiment 8) were supercritical releases at around 150 bar pressure and 150 ^{o}C temperature. The release nozzle in both the cases measured ½".

A figure of the storage and release system is shown below:

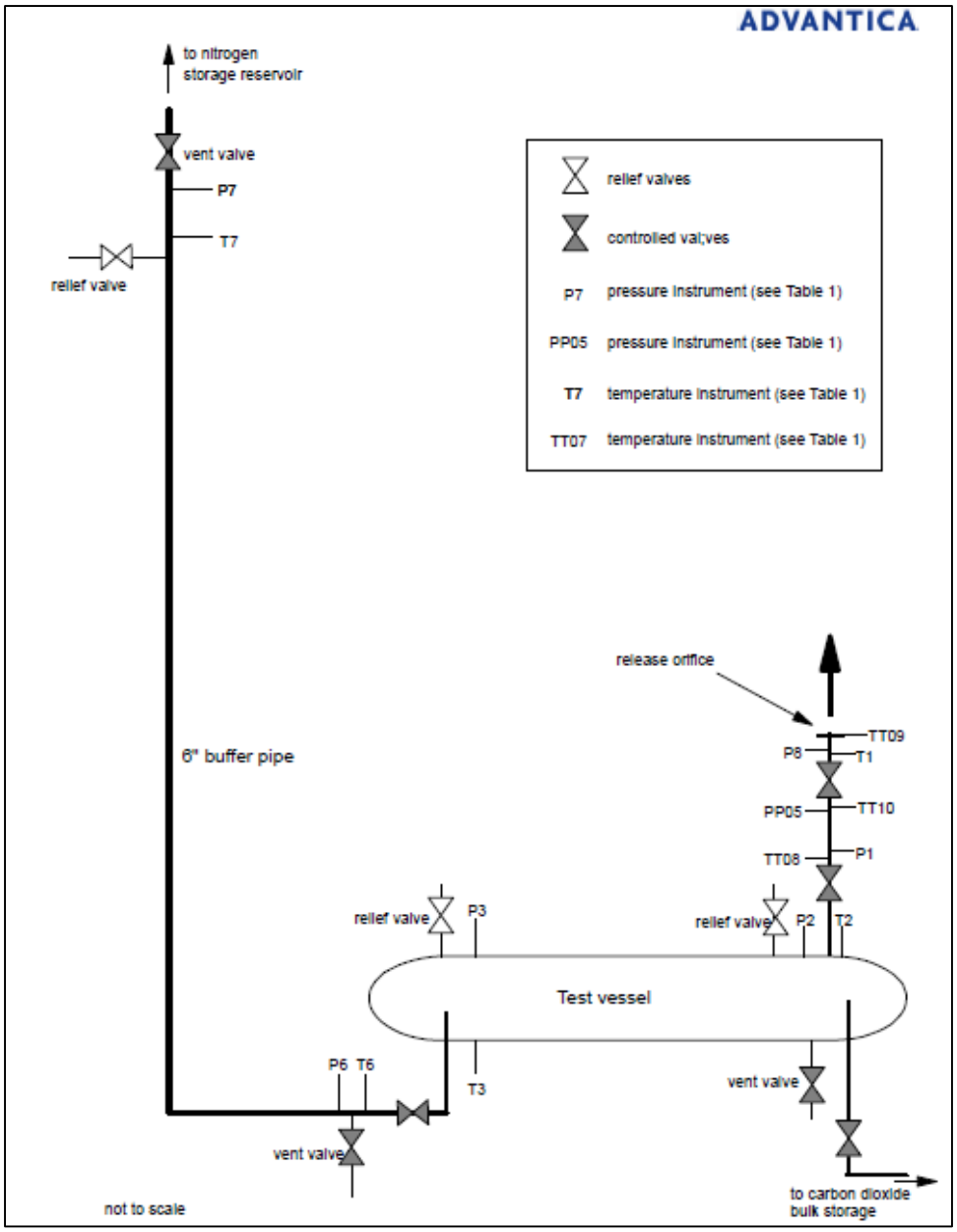

Figure 12: Experimental setup of the components at the test rig (DNV CO_2PIPETRANS Joint Industry Projects 2012)

The experimental setup comprised of a test rig 100 m x 100 m that was constructed on the Spadeadam site. The test rig consisted of a cylindrical release vessel of length 24 m and 0.6096 m diameter (24") with a total volume of 6.3 m^3 welded on both the sides. The test fluid was heated to the desired temperature before entering the release vessel by suitable pre-heaters. The vessel was completely insulated by using an insulation material to maintain the temperature inside the vessel. Two flexible pipes were attached at opposite ends of the release vessel: one led to the release nozzle and the other led to the 6" buffer line. The buffer pipe, containing nitrogen as a medium, was used for driving the fluid out of the vessel in case of steady state releases. The nitrogen was maintained at the same pressure as the CO_2 in the vessel and was injected from the opposite end to push the CO_2 out of the vessel. Experiments 8 and 8R were transient releases and pressure was used as a driving factor for CO_2 release in this case, hence no buffer was used. The high pressure conditions inside the vessel were released at ambient conditions through a release nozzle. The release pipework was attached to the vessel through two valves. The first was connected from the vessel outlet to the flexible pipework and the other led to the release pipework. The release orifice was drilled through a flange of size approximately 47.8 mm and could be changed as per the requirement. In the present case, the orifice was an 11.94 mm diameter hole.

The release orifice was taken as the origin and the release direction was aligned along the X-coordinate. The release nozzle was placed at 1.1 m above ground. All instrumentation for measuring the gas pressure, temperature, concentration etc. were placed along the X-axis at different angles and distances from the orifice as shown in figures 13 and 14.

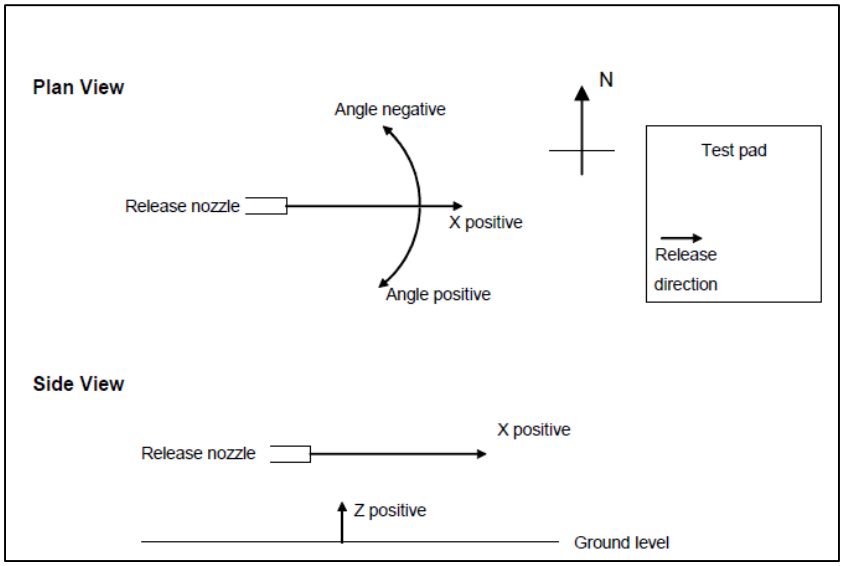

Figure 13: Orientation of the nozzle orifice with respect to the coordinate system (DNV CO_2PIPETRANS Joint Industry Projects 2012)

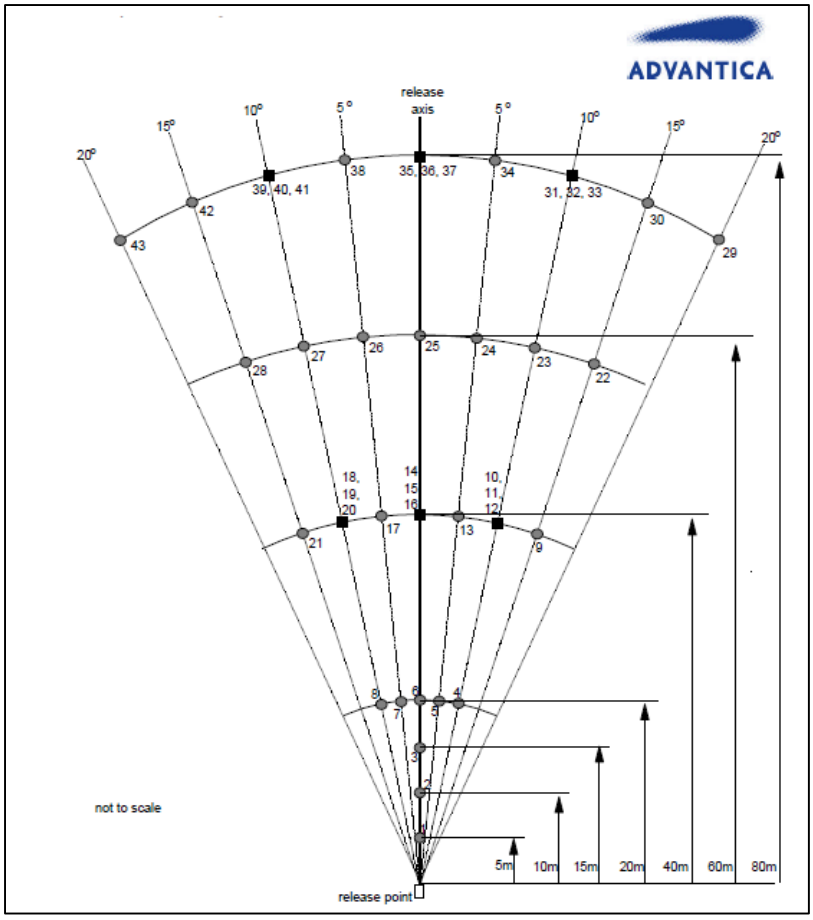

Figure 14: Instrument layout at different distances from 5 m to 80 m in the x-direction (DNV CO_2PIPETRANS Joint Industry Projects 2012)

Wind speeds were measured at different heights from the ground at 3.25m, 5.05m and 8.55m at a distance 17.2 m from the release orifice point by wind speed anemometers. Concentration measurements were made at distances 5m, 10m, 15m, 20m and 40m from the nozzle exit and at various angles as shown in the diagram above as the plume expanded away from the source. A clear picture of the placement of oxygen cells for concentration measurements is shown in the figure 15, below.

Figure 15: Placement of gas concentration instrumentation in the test rig (DNV CO2PIPETRANS Joint Industry Projects 2012)

In order to qualitatively analyze the samples of any solid drop off were done by placing aluminum trays at 8 different locations in the vicinity of the release nozzle.

A brief summary of the experimental and ambient conditions are listed in the table 10, below:

Table 10: Details of BP's Experiment 8

Parameter	Value/ Configuration
Release orientation	Horizontal
Release orifice diameter	1/2" (11.94 mm)
CO_2 pressure in the vessel at the beginning of the experiment	157.4 bar
CO_2 temperature in the vessel at the beginning of the experiment	148.1 ^oC
Wind speed at heights 8.55m, 5.05m, 3.25m respectively	5.5 m/s, 5.2 m/s, 4.9 m/s
Atmospheric pressure	0.96 bar
Atmospheric temperature	7.8 ^oC
Solid drop out	None
Release time duration	121 sec

3.2 Assumptions Considered for Modeling:

1) Pure CO_2 is considered in the inventory. No impurities are taken into consideration.
2) Pipe is assumed to be insulated from outside. Hence, there is no heat transfer occurring between the pipe wall and the fluid (CO_2). This is reasonable since majority of the heat is transferred between the fluid to the pipe wall during the depressurization process and the fluid flow is turbulent in this region.
3) Short section of the pipe of length 5.98 m is considered for design where the maximum impact of the changes occurring upstream of the pipe are captured in case of a decompression. Beyond this point it is assumed that the pressure propagation would be same. Also, immediately after there is a leak, the phase changes would be same as that at the intact end.

4) Since a small section of the pipe is considered, frictional effects can be neglected. It is assumed that the pressure drop in the pipe is all converted into kinetic energy of the fluid. Hence, at critical mass flow conditions, the change in the release rate with respect to change in pressure is zero.
5) Homogenous equilibrium model is considered between the vapor and the condensed phase from the nozzle exit to the end of the depressurization zone. This means that below the critical point, the liquid and the vapor share the same velocity and temperature and the point always lies on the saturation line. This fixes the temperature for a given constant pressure of the mixture at saturated conditions of 194 K at 1 atm.
6) Witlox, Stene et al. (2011) have concluded that the concluded that the presence of water vapor in the dispersing plume have limited effect on concentration measurements in the far-field. Hence, water vapor or moisture condensation has not been included for design purposes.
7) Friction and heat transfer from the liquid to the surroundings is neglected within the depressurization zone.
8) No air entrainment is assumed in the depressurization zone. This is because the jet velocity is very high and the pressure of the mixture is above ambient in this region.
9) The non-vapor or the solid fraction after the nozzle exit is assumed to be insignificant. This is due to the fact that the particle diameter of the solids or dry-ice forming post the leak is so small and velocity of the jet is so high that all the solids sublime inside the jet and there is no solid rainout or fall off on the ground. This is true for small and medium leakages and doesn't hold good for large full-bore ruptures. As per the HEM assumption above, the solid or the liquid fraction is sufficiently small so that they do not interact with the gas phase turbulence (Woolley, Fairweather et al. 2013).
10) The ratio of the orifice diameter to the diameter of the pipe is sufficiently small so that no crack propagation is considered. Fracture propagation is high in case of large leaks or full-

bore ruptures where the mass flow rate when compared to the small ruptures is very high to develop a crack.

3.3 Source Term Modeling

The near-field dispersion modeling or the source term modeling, as discussed previously, captures the phase flow and the phase changes that take place across the leak up to a short distance range of 10 m. The source term parameters such as mass flow rate, temperature, distance from the nozzle exit and non-vapor mass fraction are calculated at the pseudo-source point which serve as an input in dispersion model. Homogeneous equilibrium was assumed between the nozzle exit and the pseudo source point. All simulations were carried out in Fluent software version 16.2.

3.3.1 Geometrical Setup

In the present simulation, a 2D axisymmetric converging-diverging nozzle which comprises of pipe cross-section as the convergent part and a nozzle throat expanding in to ambient atmosphere as shown in figure 16. Short section of the pipe with a length of 5.98 m and diameter 1 m was considered to take into account phase changes upstream of the pipe in case of a leak. The nozzle diameter was fixed to 11.94 mm as per the experimental setup. The nozzle throat length considered here was 20 mm. The ambient air enclosure measured 10 m x 4 m (length x diameter). A sudden decompression and expansion of the fluid at the nozzle entrance and exit planes respectively were represented by fixing the converging and diverging sections of the nozzle at 90^{o} to the horizontal axis.

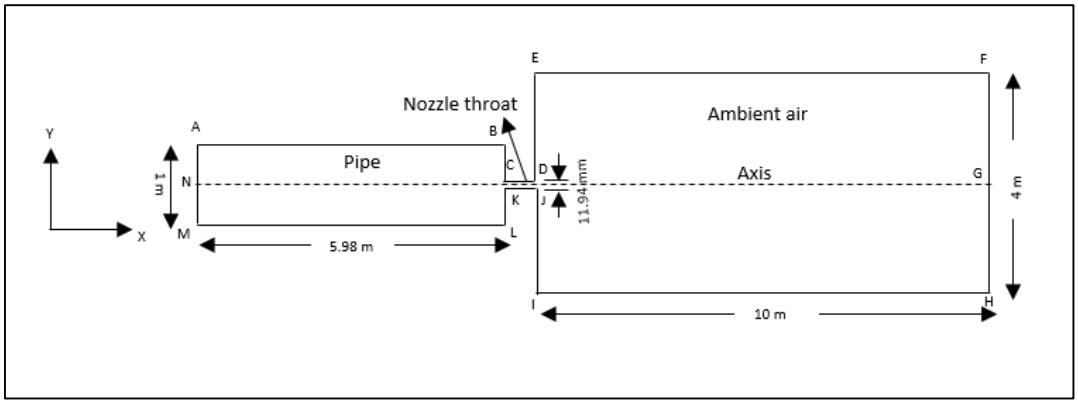

Figure 16: Schematic diagram of the 2-D computational setup for source term model (not to scale)

The material of construction considered for the pipe was steel with a thermal conductivity constant of 16.27 W/m-K for all design purpose.

3.3.2 Meshing

A very high resolution structured mesh was implemented for ensuring that the physics around the small region of nozzle throat is properly captured. This also captures the sudden changes in the gradients of the variables and takes into consideration the discontinuities in locating the Mach disk. Due to the large dimensional variation of the geometry ranging from 11.94 mm to 10 m, mesh refinement was performed and the minimum and maximum sizes of the mesh were defined to ensure that mesh was evenly distributed along all the faces and edges of the setup. The mesh contained a total of 0.41 million cells which is shown in the figure below.

All simulations were carried out in academic version of FLUENT which had a maximum cell limitation of 0.5 million cells. Hence to ensure grid independence with the given limitation, that the adapted mesh was verified at different grid sizes of 0.26 million. 0.41 million and 0.49 million. It was observed that the X-directional velocity component showed very less deviation at different grid sizes and hence an optimum mesh size of 0.41 million cells was considered keeping in view both the accuracy and the computational effort.

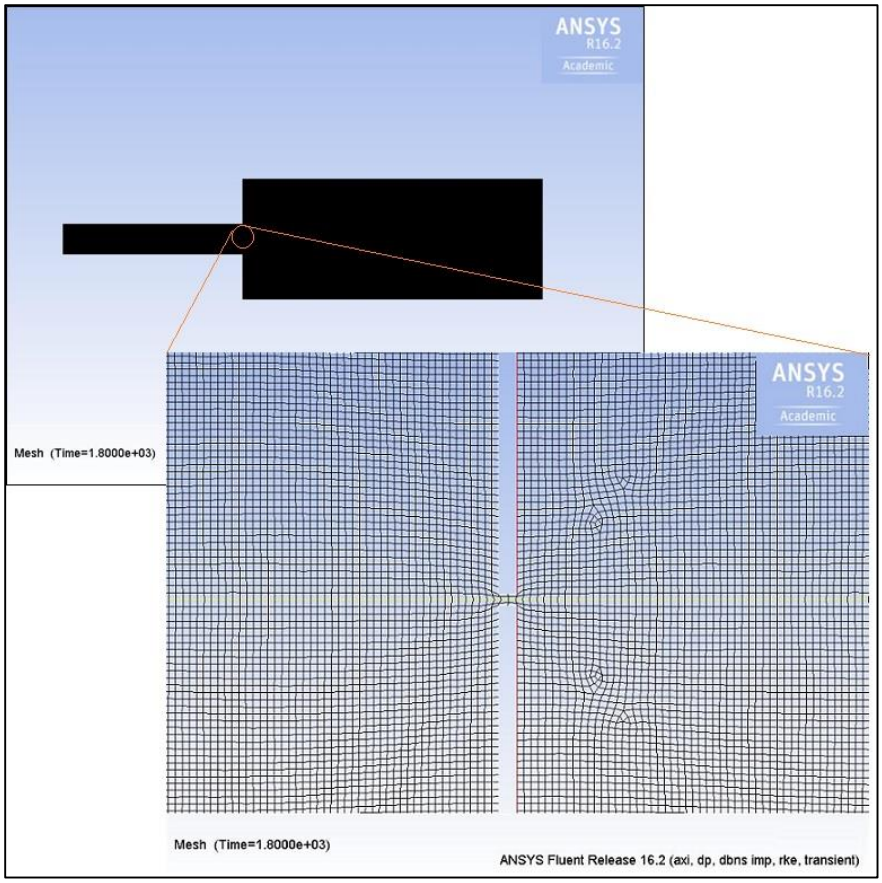

Figure 17: Mesh for source term modeling

3.3.3 Fluent Model Setup and Boundary Conditions

The fluid was initially at rest and a transient simulation was carried out for sufficient time of 1800 seconds to be considered steady state. A density-based solver to capture the shock resolution was used to depict the high speed compressible flow nature of the fluid. Realizable k-ε model was used for turbulence modeling as it gives a better prediction over the standard k-ε model in cases of adverse or very high pressure gradients. It also provides better results for the mass flow rate or spreading rate of the jet once it expands in to the ambient atmosphere.

The initial stagnation pressure and temperature was set as per the experimental conditions as 157.4 bar and 148.1 ^{o}C. Pure CO_2 was selected as the fluid in the materials section. Real gas Peng-Robinson cubic equation of state was used to define carbon-dioxide properties such as

density, specific heat, temperature, enthalpy etc. It can also accurately predict the CO_2 vapor-liquid transitions over a wide range of temperature and pressure changes from supercritical to below atmospheric conditions. Stainless steel with a thermal conductivity of 16.27 W/m-K was used as the material of construction for pipe. Boundary conditions were set at the inlet and outlet on edge AM, FH respectively on figure 16. The edges ABCDEF and HIJKLM were set as wall boundary conditions. They were defined as following:

- Pressure Inlet Boundary Condition: Stagnation pressure and temperature conditions mentioned above were set at the inlet.
- Pressure Outlet Boundary Condition: Outlet pressure and temperature were set to the ambient conditions as mentioned on the test site as 0.96 bar and 7.8 ^{o}C respectively.
- Wall boundary Condition: Stationary, no slip wall boundary condition with a default constant wall roughness of 0.5 was set. The wall was also adiabatic and insulated for any heat transfer.

An implicit second order method was chosen to define the transient formulation. The numerical simulation was solved by finite volume approach with a courant number of 0.5 for convergence of solution. The absolute criteria for convergence tolerance was set by adjusting the residual monitors to 0.001.

The pseudo source point was located at a distance where the jet reached atmospheric pressure and the corresponding mass flow rate, temperature, vapor mass fraction etc. were calculated at the exit plane.

3.4 Dispersion Modeling

The results from the source term model transient simulation were set as the initial point for dispersion model in a 3-dimensional Cartesian coordinate domain.

3.4.1 Geometrical Setup

Figure 18 depicts the computational domain for the dispersion model. The dispersion model contained a rectangular box of dimensions 100 m x 80 m x 50 m (span wise on X-axis x width wise on Y-axis x height on Z-axis). One of the YZ faces containing origin as one of the points was set as the inlet plane for wind and CO_2 inlet and the opposite face was set as outlet. One of the XY faces containing origin as one of the points was set as ground and the opposite wall was set as top wall. The other two faces with the XZ faces were treated as side faces. CO_2 inlet source was treated as a circular face with an expanded area of approx. 0.053 m^2 which is much larger than the orifice diameter in the previous model. The distance from the nozzle exit to the pseudo source point derived from the source term model approx. 0.041 m was extruded perpendicular from the inlet face into the computational domain. The CO_2 source inlet was placed at a distance of 40 m from the origin in the Y-direction and at a height of 1.1 m from the ground in the Z-direction. Since the release nozzle orientation was horizontal as per the experimental setup, CO_2 release was set parallel to the direction of wind.

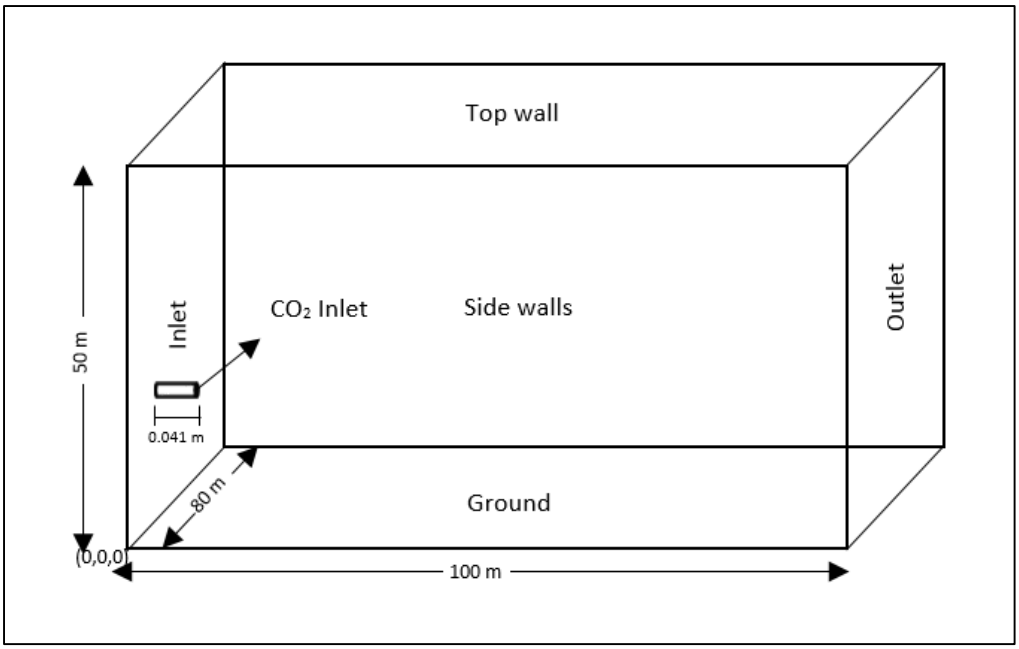

Figure 18: Computational domain setup for dispersion model

3.4.2 Meshing

Fine meshing was done along the curvature and proximity with a total of 0.51 million hexahedral elements as shown in figure 19.

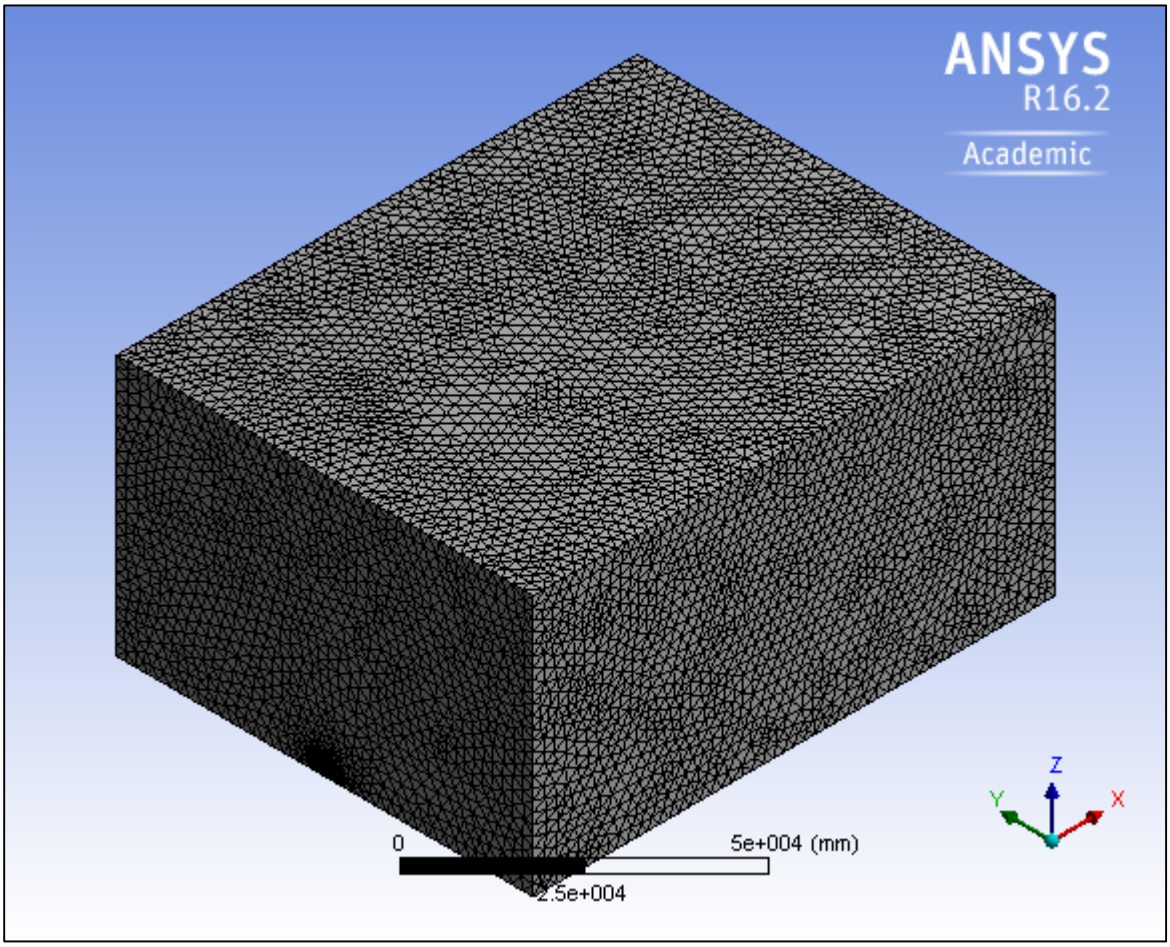

Figure 19: Computational meshing of the domain for dispersion model

The region around the pipe curvature and circular area of the source were refined by using face sizing with a minimum element sizing of 2.8 mm as shown in figure 20. This allows an unstructured mesh allocation around the source point creating sufficiently fine grid structure in the vicinity of the release pipe where maximum concentration variations take place. An appropriate orthogonal quality of close to 1 while a skewness close to zero ensures good quality meshing and prevents sudden decrease in the mesh density at a certain point. In contrary, Adaptive Mesh

Refining (AMR) can be implemented which automatically refines the mesh in the areas of steep gradients near the fluid flow allowing the process parameters to define the density of mesh.

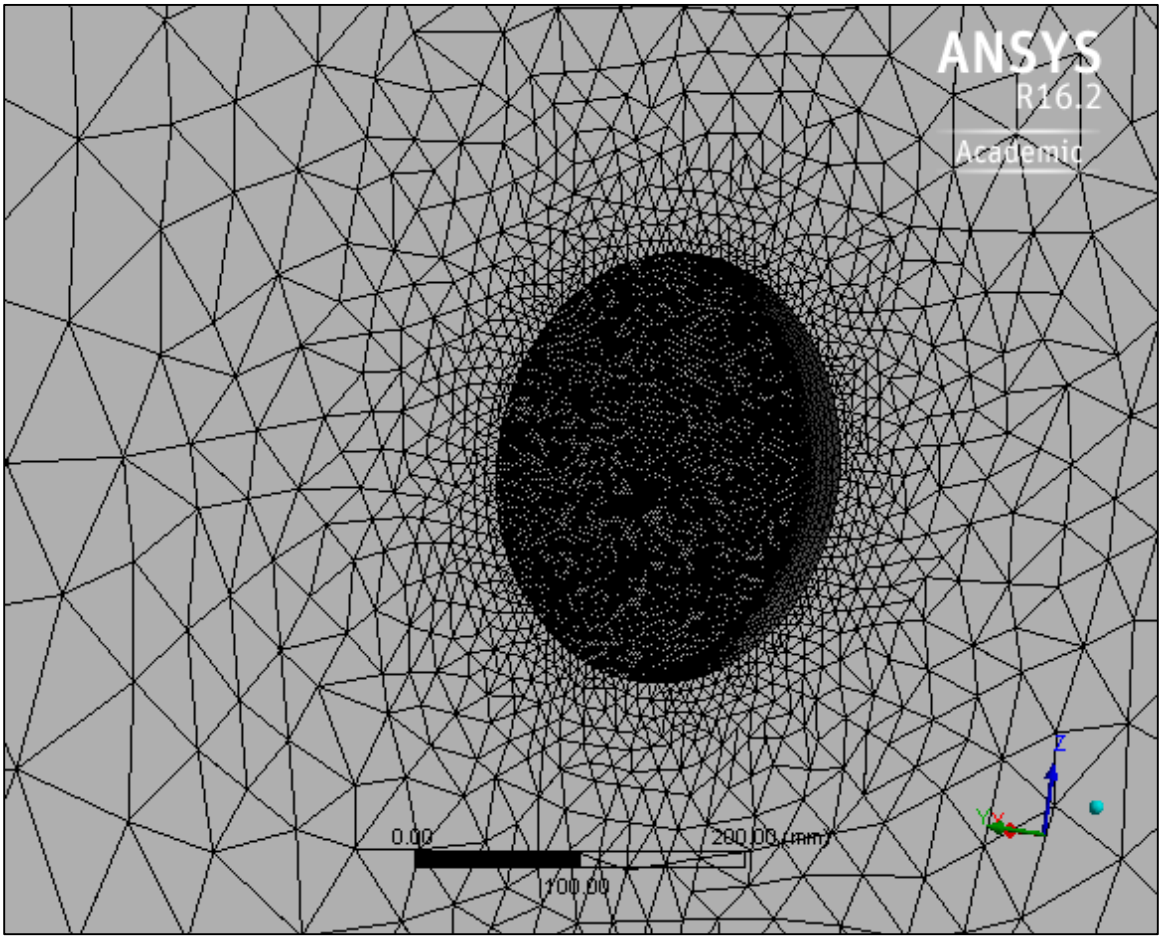

Figure 20: Refined mesh around the CO_2 source inlet

3.4.3 Computational Setup and Boundary Conditions

A pressure-based solver was used to carry out both the steady and transient simulations in the dispersion model. Gravity was specified along the negative Z-axis. Fluent simulates the turbulent atmospheric dispersion of pollutants via Navier-Stokes equations. A viscous k-ε turbulence model was used with standard wall functions to close the set of RANS equations as well as to study the viscous dissipation and buoyancy effects of the surrounding atmosphere. The discrete equations for mass, momentum and energy along with the k-ε equations is solved in a finite

volume method. The wind velocity profile was defined by the power-law correlation where the mean velocity at a certain point was determined by the $'\alpha'$ power of its height as per equation 13, shown below:

$$\frac{\bar{U}(z)}{U(H)} = \left(\frac{z}{H}\right)^{\alpha}$$

The wind velocity was input in the form of a user-defined input in the boundary conditions. The reference values of mean wind velocity, $U(H)$ was given as 5.2 m/s at a height of H=5.05 m. A detail UDF code for the wind velocity profile input is given in Appendix-A.

The stability class selected was neutral class D with the given wind speed, cloud cover and solar radiation data available from the experiment.

The model was initially operated at steady state condition to obtain a uniform wind profile inside the computational domain when there was no CO_2. This was done by setting the CO_2 source as 'wall' initially and a converged solution was obtained at 88 iterations. Then, a transient simulation was carried out for 121 seconds by initializing the run with the above converged solution and turning the CO_2 input to 'mass flow rate' boundary condition. This creates a fully developed atmosphere inside the domain before injecting CO_2 and allows accurate prediction of pollutant dispersion in far-field.

Although the mass fraction of the solids was high, the volume fraction of solids at the pseudo source plane was minimal. Hence, a homogeneous equilibrium model was implemented and a constant enthalpy was assumed between the nozzle exit plane and the pseudo source plane. The required average non-vapor mass fraction was calculated from the source term model and implemented at the CO_2 source in the present dispersion model. The homogeneous model assumption states that for a two-phase flow, the vapor and the condensed phases are always in equilibrium below the critical point and the path taken for the decompression always lies on the saturation line. Also, the slip between the two-phases (or the difference between the velocities and

temperatures) is assumed to be negligible. This fixes the pseudo source point temperature at 194 K (at a constant pressure of 1 atm ambient pressure). This is a good assumption due to two reasons.

1. The region of expansion from high pressure to atmospheric pressure is very small in comparison to the actual geometry (in this case, 0.041 mm).
2. The density ratio between the condensed phase and the vapor phase is close to unity ($\rho_{liq}=\rho_{vap}\cong 0.4641$ g/cc) as the two-phase fluid is close to critical point and hence, it is safe to assume insignificant slip between the phases.

Since the model involved only vapor CO_2 and air, no multiphase volume of fluid method was required. Species transport model was selected with a mixture of CO_2 and air. Peng-Robinson equation of state was used to define the properties for dense gas dispersion. The mass flow rate of CO_2 at the inlet can be evaluated from the average density and velocity calculations at the exit plane in y-direction by the formula below:

$$\dot{m} = \frac{A_s}{N}\sum_{i=1}^{N}(\rho_s)_i(v_s)_i \qquad (\mathbf{19})$$

where $\rho_s =$ density of the fluid on the pseudo-source plane (kg/m^3)

$v_s =$ velocity of the jet on the pseudo-source plane (m/s)

$A_s =$ area of the circular pseudo-source (m^2)

$N =$ number of points considered on the vertical jet axis

The pseudo-source was input as a circular pipe opening in dispersion modeling with a radius equal to the vertical height of the plume from the axis. The horizontal distance of the pipe was based on the distance calculated from the nozzle exit to the point where the jet first reaches atmospheric pressure.

Since, homogeneous equilibrium was assumed between the orifice exit and until the jet reached atmospheric pressure, the corresponding saturated temperature at atmospheric pressure was fixed to 194 K.

The vapor mass fraction was achieved by assuming isenthalpic conditions in the depressurization zone. If a control volume is constructed around the nozzle exit plane (b) and the pseudo-source plane (a) in figure 11, the energy balance equation along the axis in 1-D can be replaced with the enthalpy balance equation as follows:

$$h_{mix\,(exit)} = h_{solid\,(s)} + \beta\left(h_{gas\,(s)} - h_{solid\,(s)}\right) + \frac{1}{2}u_{(s)}^2 \qquad (\mathbf{20})$$

where $h_{mix\,(b)}$ = enthalpy of the mixture at nozzle exit (J/kg-K)

$h_{solid\,(s)}$ = enthalpy of solid at pseudo-source point (J/kg-K)

β = vapor mass fraction of CO_2

$h_{gas\,(s)}$ = enthalpy of gas at pseudo-source point (J/kg-K)

$u_{(s)}$ = velocity at the pseudo-source point (m/s)

A total of five boundary conditions were defined: wind inlet, CO_2 inlet, outlet, ground, top and two sides.

- Wind Inlet: A velocity inlet was defined along the positive X-axis and a constant wind velocity of 5.51 m/s was selected as input. A separate case study was also carried out for variation of the dispersed gas pollutant concentrations under power law wind velocity profile conditions by reading the UDF into the velocity magnitude section. Ambient temperature was set as per the experiment at 281 K.
- CO_2 inlet: A mass flow inlet was specified along the positive X-axis and the average mass flow rate and vapor mass fraction of 3.4274 kg/s and 0.887 respectively obtained at the pseudo-source plane from the previous model was given as the input. The temperature of the source was given as 194 K.
- Outlet: A pressure outlet boundary condition was set with the pressure and temperature at ambient conditions.
- Top and Two Sides: The top wall and the side two walls were defined together as symmetry boundary condition which assumes no shear slip at the walls and the normal flux across

the wall to be zero i.e. the velocity conditions at the wall are taken from the node immediately adjacent to the wall.

- Ground: Wall boundary condition was defined at the ground with a constant wall roughness of 0.5 and no shear slip.

The pressure and velocity fields were coupled in the Navier-Stokes equation and the spatial gradients were discretized by using second order upwind. The simulation was carried out until the tolerance criteria of 0.001 was met for the residual monitors.

3.5 Study of Gas Dispersion in the Presence of Obstacles

A series of 3-dimensional rectangular blocks of obstacles of dimensions 10 m length x 10 m width x 2 m height were placed at different distances from the CO_2 source in the computational domain in order to investigate the behavior of the pollutant in the presence of obstacles such as buildings or trees in the vicinity of the leak. One of the obstacles was placed at a distance of 8 m from the source while the other two were placed at a distance of 20 m from the source as shown in figure 21. Fine meshing was done on the ground where the obstacles were present when compared to other parts of the domain as shown in the figure 22. Constant wind inlet velocity of 5.51 m/s was introduced and standard k-ε model was selected to define turbulence.

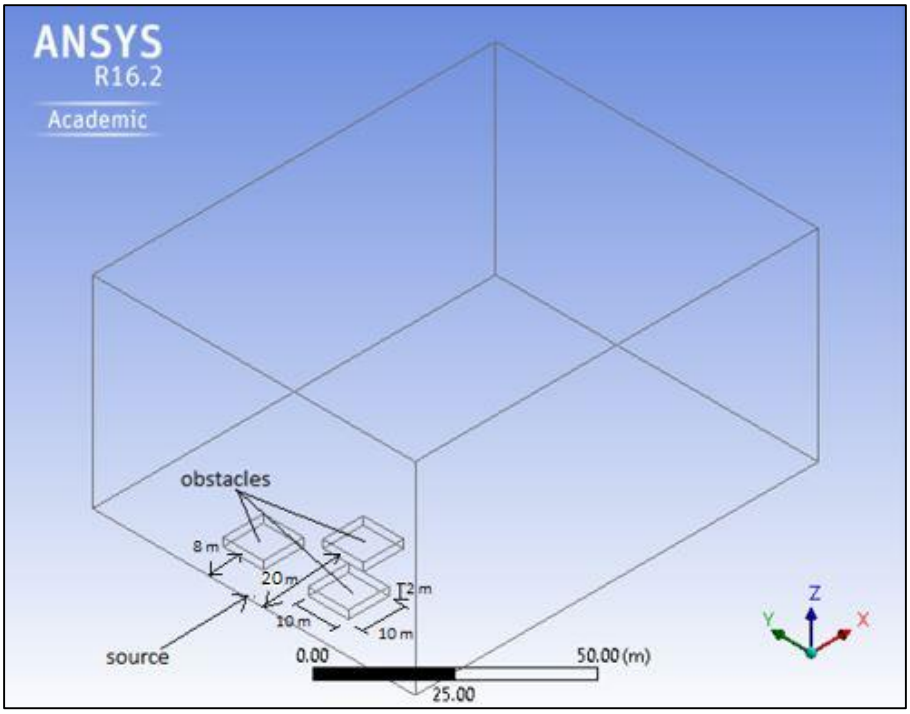

Figure 21: Geometrical setup of the computational domain in the presence of obstacles

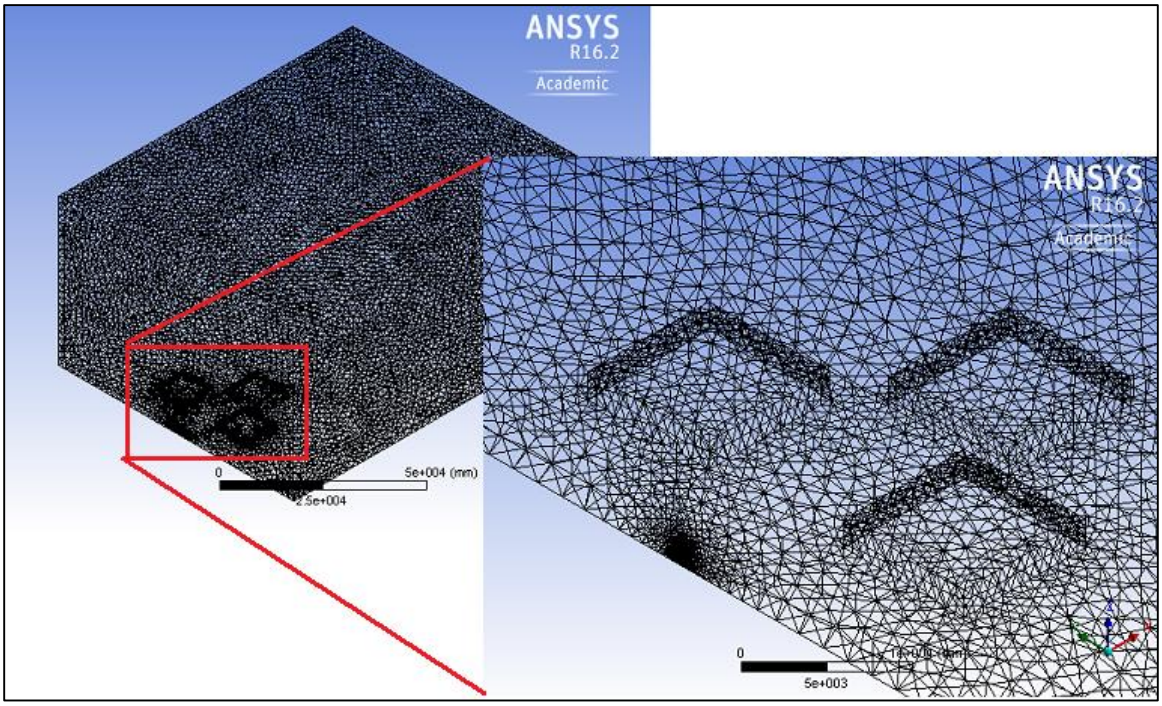

Figure 22: Computational mesh for the domain in the presence of obstacles

A steady state simulation was carried out to establish a constant wind field inside the domain before starting the transient simulation. The steady state simulation converge at 90 iterations. A transient simulation was carried out to track the change in concentration in a period of first 20 seconds after the leak. Mass flow rate and other boundary conditions were kept similar to the base case scenario.

CHAPTER IV

RESULTS AND DISCUSSION

4.1 Mach Disk Location

Simulations were carried out to study the behavior of the jet in the near-field model up to 10 m in ambient air. The stagnation pressure and temperature selected were as per the experimental conditions of 15.74 MPa and 420.3 K respectively. The evolution of the under-expanded free jet from an orifice of diameter ½" was studied. The high pressure gas discharge through the nozzle interacts with the atmosphere to create a series of compression and expansion waves in the form of oblique shocks which can be viewed in the figure 23. This flow structure is in close resemblance with the jet flow through nozzle conditions from literature as shown in the figure 9.

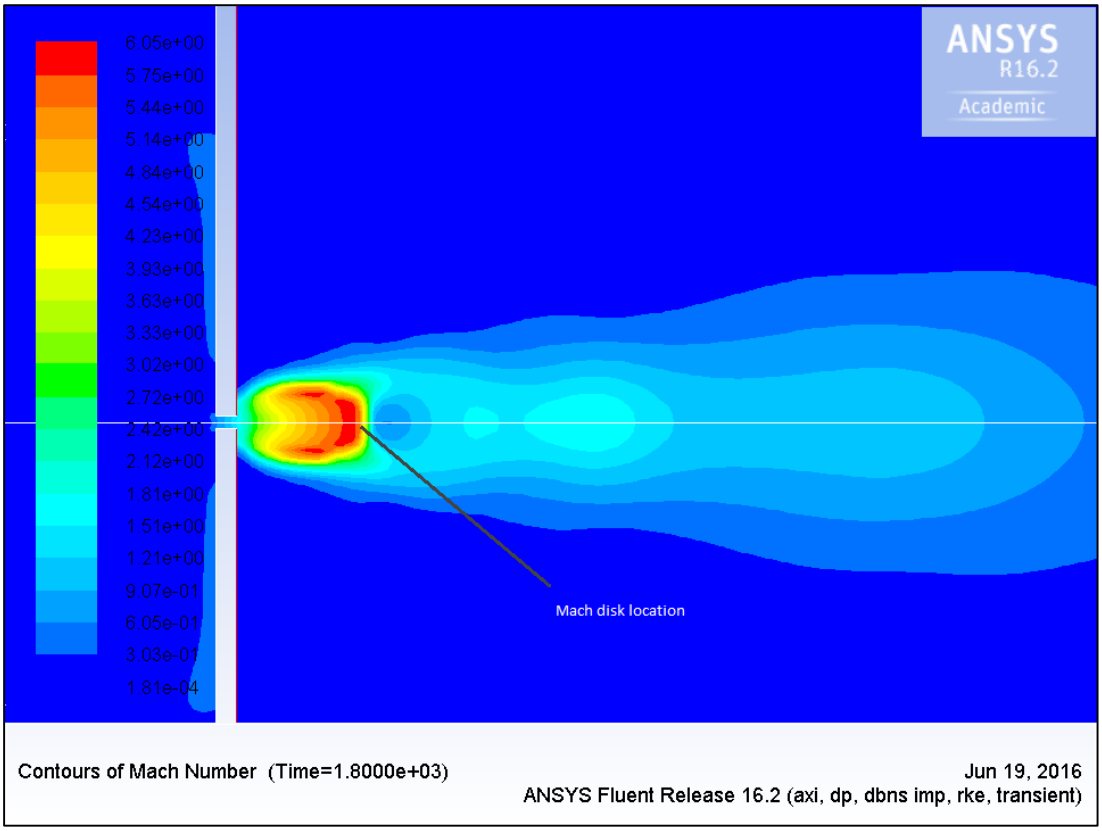

Figure 23: Contours of Mach number

When the incompressible fluid comes in contact with the atmosphere in case of a leak, the fluid can be treated as compressible fluid. Realizable k-ε turbulence model gives better results for the flow structure near the nozzle leak and hence can be preferred over the standard k-ε model. The effect of the location of Mach disk to the pseudo-source point was analyzed and it was observed that the Mach disk is located at a distance of approximately 0.113 m which is 9.5 orifice diameters from the orifice exit. However, the series of pressure waves generated post leak reach a stable constant ambient pressure at a distance of approximately 0.142 m from the nozzle exit which is 11.9 times orifice diameters. Hence, from the above results, a general rule of thumb to locate the minimum distance of pseudo-source point from the nozzle exit would be roughly 1.25 times the Mach disk location when the stagnation pressure and temperature match the current case

conditions. This is especially helpful in cases where the mathematical method is zero-dimension or cannot predict the distance to be employed for far-field modeling.

The Mach disk location varies from case to case and is usually a function of the stagnation pressure. The Mach disk location increases when the initial pressure increases. Peng Robinson equation of state gives good prediction of the pseudo-source and Mach disk location from nozzle exit by accurately varying the density over the wide range of temperature changes from 420 K to less than 173 K in the geometry.

4.2 Source Term Simulations

4.2.1 Mass Flow Rate

Figure 24 shows the variation of the transient mass flow rate at the nozzle exit. For time-varying releases, the discharge rate is calculated by time-averaging the mass flow rate for 20 seconds time interval. From the graph we can see that the average release rate gradually decreases over the period of 121 seconds. There is not significant decrease in the mass flow rate characteristics but the average mass flow rate is correctly predicted. The average mass flow rate as per the experiment during the transient release was 3.39 kg/s while the calculated values predicted from the source term model at the pseudo-source location by FLUENT was 3.427 kg/s. The % error in the prediction is +1.09%. This slight overestimation can be used to design a conservative approach for estimating the worst case scenario in dispersion modeling.

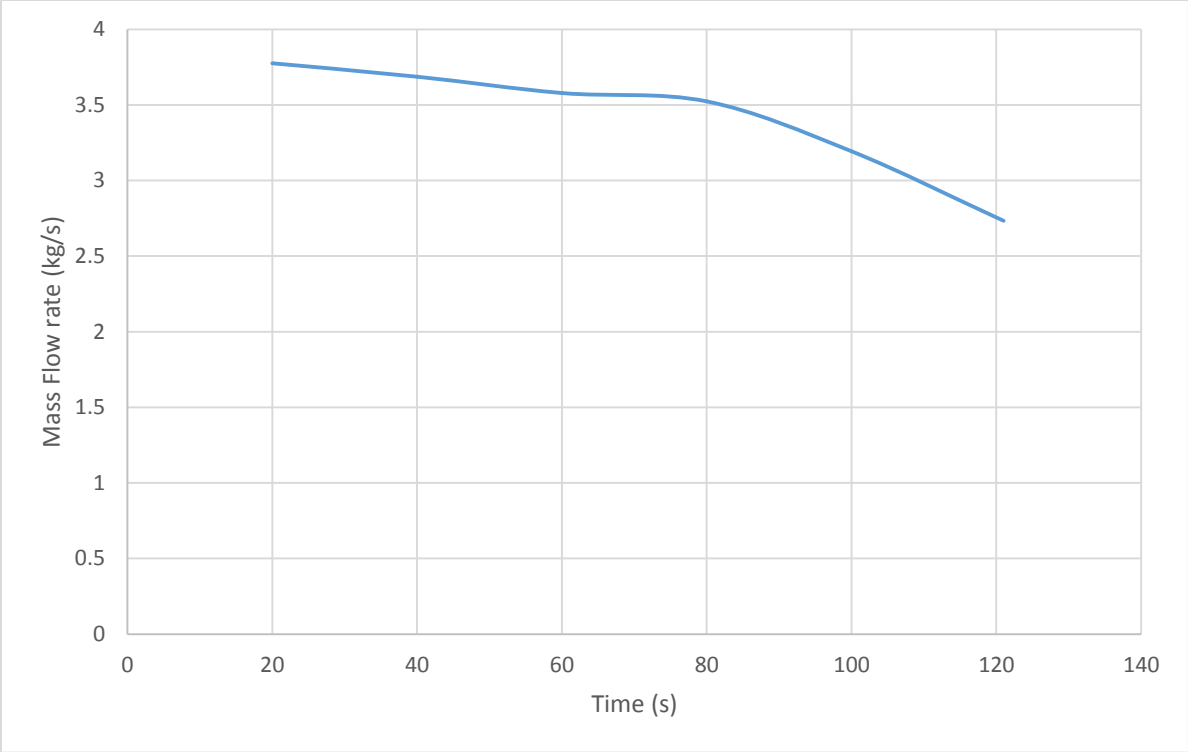

Figure 24: Time-varying discharge rate trend

Table 11: Mass flow rate values for 20 seconds time-averaging

Time (s)	Mass Flow Rate (kg/s)
20	3.776
40	3.687
60	3.579
80	3.523
100	3.193
121	2.733
Average from Calculations	3.427
Average from Experiment	3.39
% Error = +1.09	

If we calculate the amount of mass initially present in the vessel,

Volume of the tank initially (V_0) = 6.3 m^3

Density at initial pressure (157.4 bar) and temperature (148.1 ^oC) (ρ_0) = 250.13 kg/m^3 (Span and Wagner 1996)

Total mass = $V_0 \rho_0$ = 1575.8 kg

In case of a leak, at the estimated flowrate of 3.427 kg/s, a total of 414.7 kg of mass would get empty in a duration of 121 seconds. This is almost 26.3% of the total inventory which would get empty in first 121 seconds. At this rate the entire tank would be empty in a duration of 8 minutes. If proper check valves and arrestors are not present, the gas diffuses up to larger distances causing greater damage.

4.2.2 Dry-Ice Formation

Figure 25 shows the predicted contours of temperature for transient expansion of the nozzle in the 2-D plane towards the end of 1800 seconds. The pressure in the entire region after nozzle exit is ambient pressure (1 atm). It can be clearly viewed that the temperature falls much below 173 K post expansion just prior to reaching the Mach shock location. In this region, the entrained liquid droplets are condensed into solid particles of CO_2. Near the vicinity of the leak, due to insufficient entrainment of ambient air, majority of the sublimation of solid particles takes place. Liquid droplet evaporation takes place in this region by drawing heat from the surrounding warmer vapor molecules, further decreasing the temperature of the mixture.

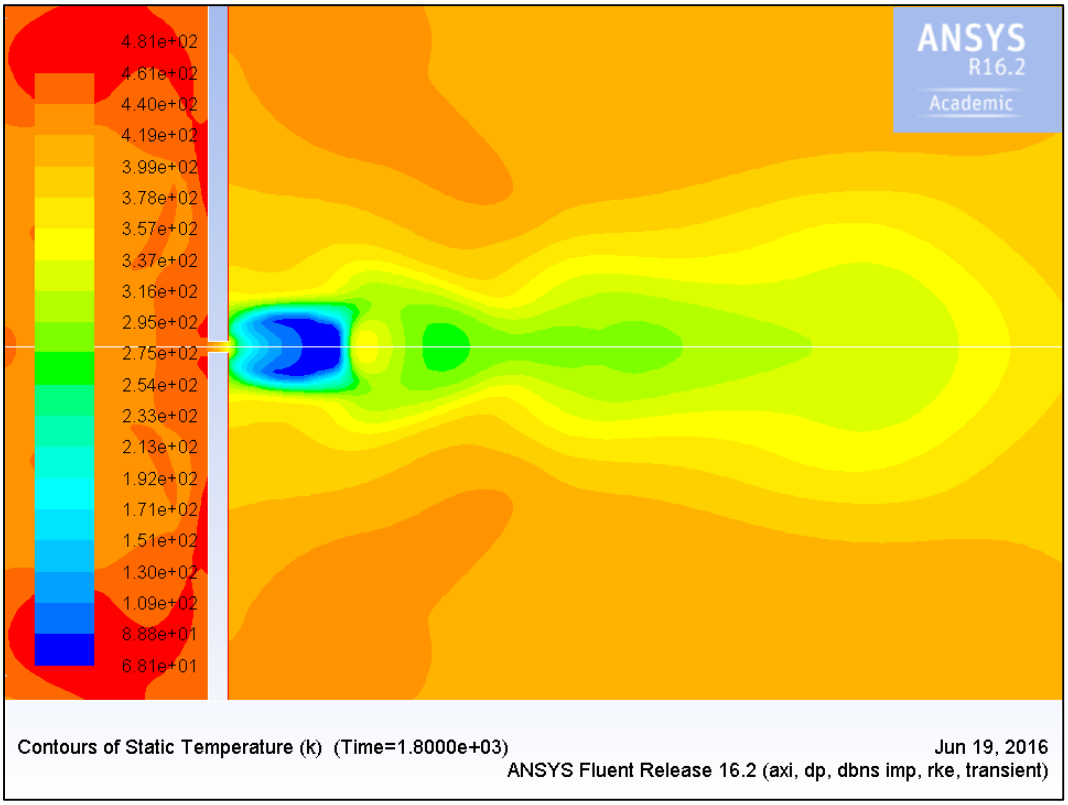

Figure 25: Contours of temperature post nozzle expansion into ambient air

Since homogeneous equilibrium is assumed in the depressurization zone, the vapor and liquid are always assumed to be in thermal equilibrium for a pure CO_2 case. Therefore, once the jet reaches atmospheric condition, a saturation temperature of 194 K was assumed. It can also be observed that all solid formation was in the expansion zone and no solid formation was observed within the pipe. This also eliminates the possibility of fracture propagation due to solid accumulation within the pipeline. The solids are formed only up to a few millimeters after the orifice exit such that entire solid sublimation takes place within the jet and there is no solid rainout on the ground.

4.2.3 Velocity Magnitude post Mach Shock

The velocity was highest at the Mach shock location with a value of almost 774 m/s which can be viewed in the figure 26. The nozzle exit is located at 6 m from the inlet and there is a sudden jump of velocity at the Mach shock. The velocity of the jet was observed to gradually decrease once it reaches the entrainment zone and reaches to a constant value as low as 9 m/s.

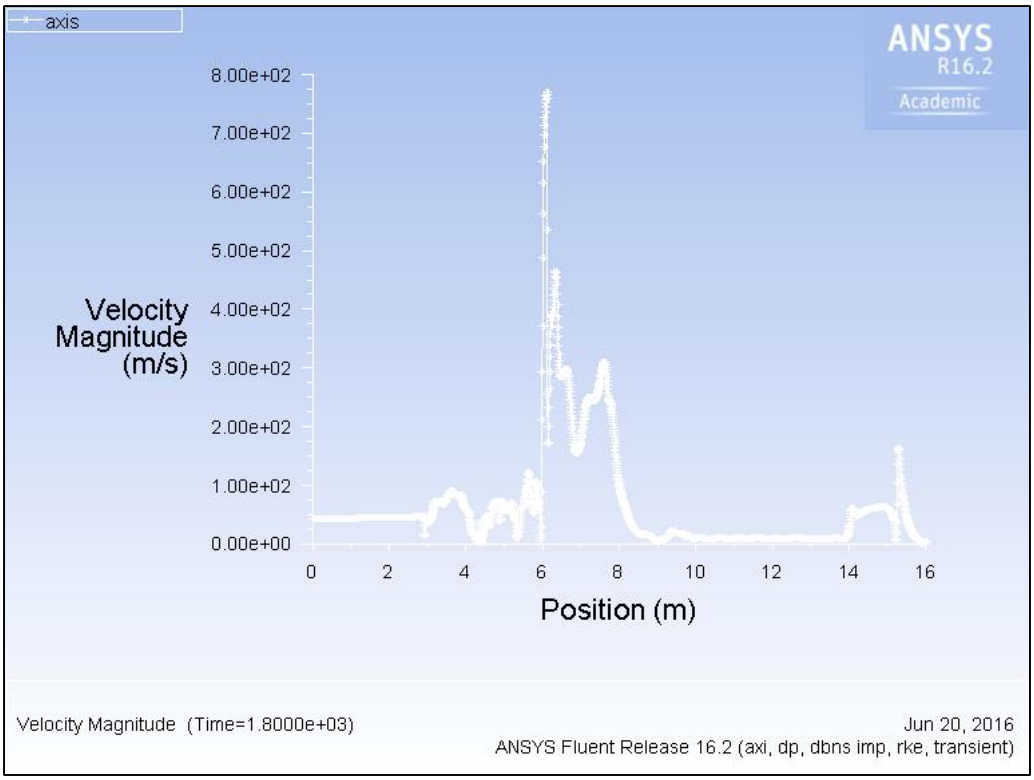

Figure 26: Variation of velocity along the jet axis

The emerging liquid at a distance of 0.01312 m from the orifice exit is initially in liquid state which rapidly flashes into the solid-vapor state due to the large superheat it contains. At this stage, the mixture contains liquid aerosol droplets in vapor CO_2. There is a possibility of the presence of finely-dispersed CO_2 solid particles which finally increase in number due to the additional condensation of liquid droplets. The density of the mixture is very high and it was

observed that at this point the density is almost 29.7 kg/m^3 which is almost 24 times that of ambient air.

4.3 Dispersion Modeling

4.3.1 Concentration Fluctuations and Time-Averaging

Determining concentration fluctuations over a certain distance downwind forms the major hazard assessment tool when dealing with constantly varying atmospheric dispersion. For instance, the concentration measured by the sampler at a distance 5m downwind from the release, might not be the same in the first 10 seconds versus in the first 20 seconds. Evaluating these concentration variations over the given transient release will allow us to determine whether the fraction of CO_2 concentration has exceeded the minimum specified threshold levels.

Once the jet has entrained sufficient air is in the entrainment zone, the source strength begins to gradually decrease over distance and it is observed that after a specific distance, the jet begins to meander when it attains the velocity equal to the wind velocity. Turbulence plays a vital role in determining the amount of vertical plume dissipation in ambient air. The uncertainty in the wind speed and direction also causes CO_2 plume concentrations to fluctuate along the centerline for a short duration of time, thus causing the monitor to detect higher concentration readings for a few seconds. Hence there are peak concentrations (maxima and a minima) recorded at some instances of time.

In order to trace the short term fluctuations, a mean concentration variability is calculated along the plume centerline over a fixed time iterations of T. This is known as time-averaging. The continuous concentration readings recorded by the experiment are divided into short time intervals. Fluent allows data sampling for time statistics which calculates the mean concentrations over a 20 seconds time interval. The sampling time for time averaging is selected such that it is large enough to capture the peak concentrations as well as the time scales of random eddy motions. The time averaging concentration for a given time t is defined as:

$$\bar{\chi}_T(t) = \frac{1}{T}\int_{t}^{t+T} \chi(u)du \qquad (\mathbf{21})$$

where $\bar{\chi}_T(t) =$ time averaged concentration (ppm)

$\chi(u) =$ instantaneous concentration (ppm)

The experiment 8 for BP was carried out for a total time of 350 seconds and the release was initiated at 90.5 seconds and lasted for a duration of 121 seconds. The CO_2 concentration measurements were carried out at 5 different locations 5 m, 10 m, 15 m, 20 m and 40 m downwind form the release. Concentration time averaging was done at a 20 seconds time interval for the entire release along the plume centerline. This gives us the mean value snapshot of the concentration over the entire 20 seconds duration of release. The mean wind speed considered for this experiment was 5.51 m/s along the positive X-direction.

4.3.2 Case Study: Effect of Wind Velocity Profile on the Concentration Variations

For FLUENT simulations, an inlet mean wind velocity of 5.51 m/s for the actual case was based on the mean reference velocities recorded by the anemometer close to the nozzle prior to the release from the experiment. The power-law correlation was based on the constant wind velocity profile based on a reference wind velocity for the entire computational domain.

A case study was performed by varying the wind profile over the computational domain using wind power law-correlation as stated in equation 13. This is based on reference values of 5.2 m/s wind velocity at a height of 5.05 m from the ground. The wind profile was simulated by interpreting user-defined function (UDF) using C program into the FLUENT software. This takes into account the wind shear and turbulence in the vertical direction, thus giving an accurate plume concentration at various heights.

Figures 27 to 31 give us the time averaged concentrations predicted by Fluent versus the experimentally recorded values. The graphs predict a good agreement of the mean concentrations

over the entire release duration. The maximum peak concentration is recorded well by the software and hence, the given sampling time interval of 20 seconds is able to capture the maximum values observed during the experiment. Although the concentration levels are overestimated at 10 m, 15 m, 20 m and 40 m, this is good from the perspective of hazard assessment tools for predicting the maximum threshold levels.

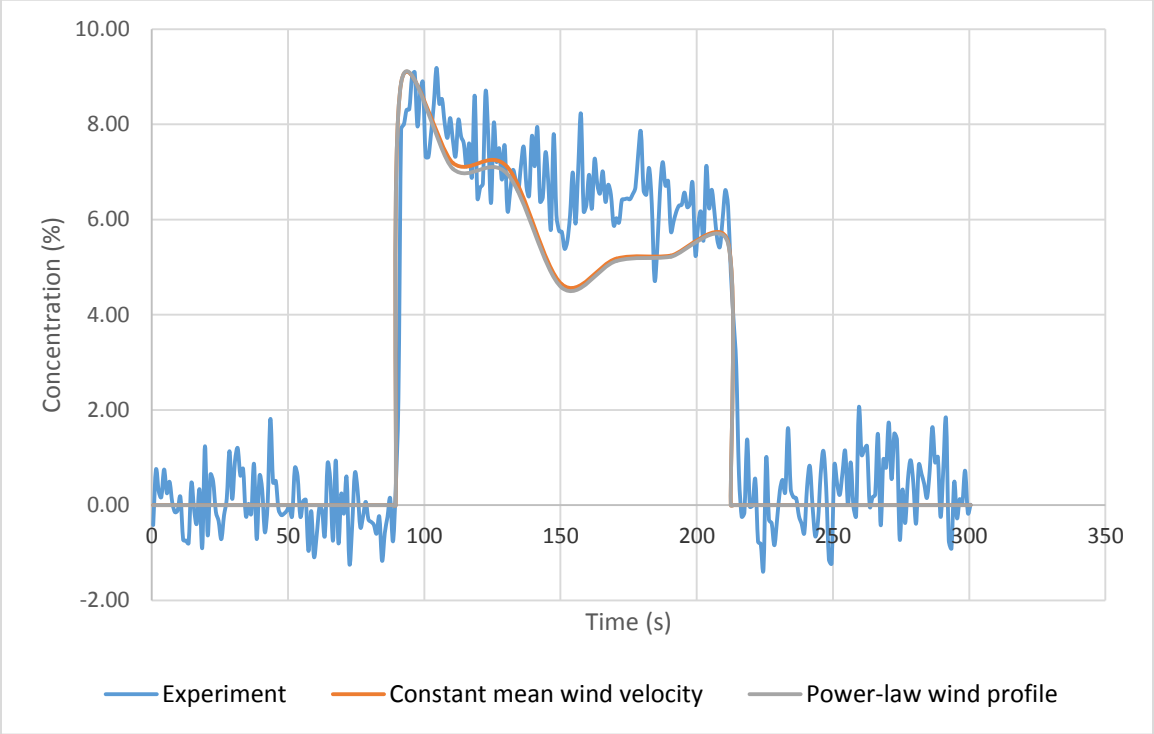

Figure 27: Concentration variations with time at 5m downstream from release point

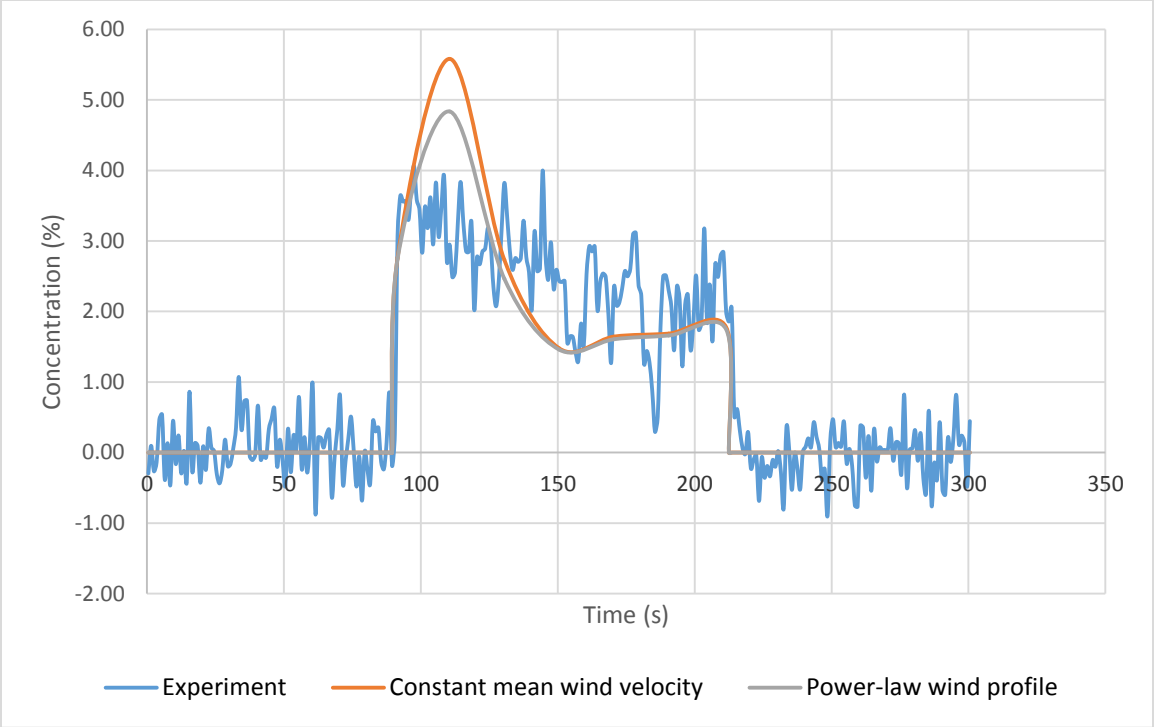

Figure 28: Concentration variations with time at 10 m downstream from release point

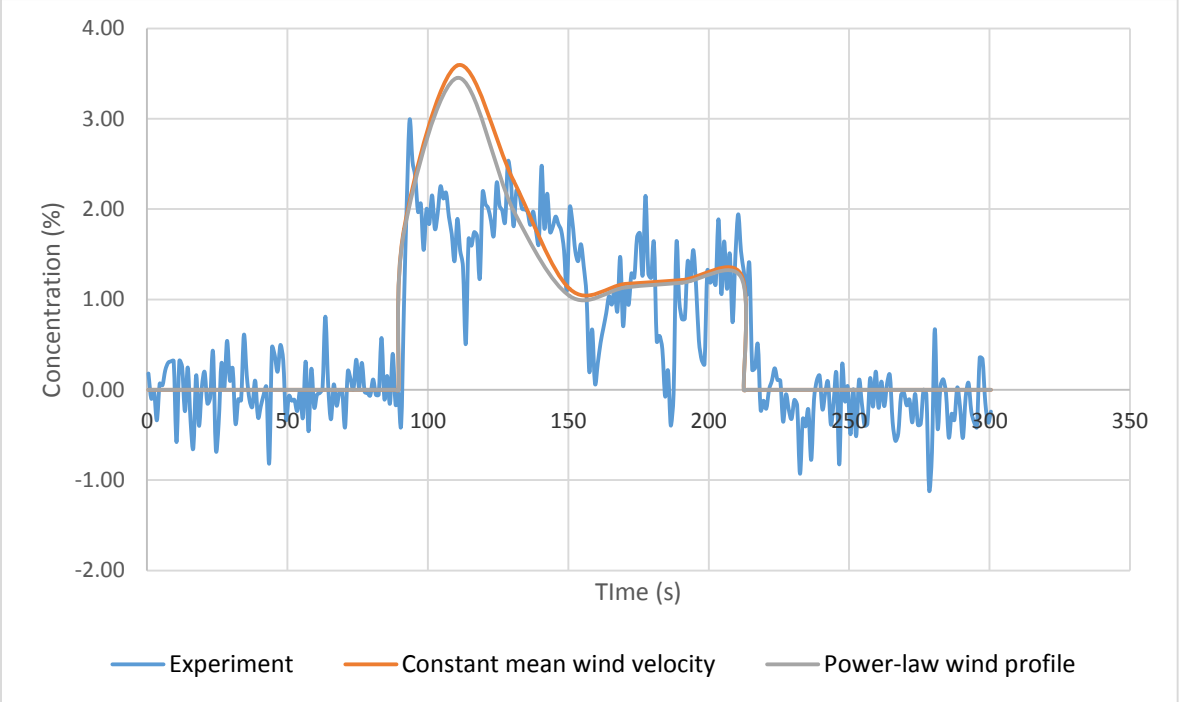

Figure 29: Concentration variations with time at 15 m downstream from release point

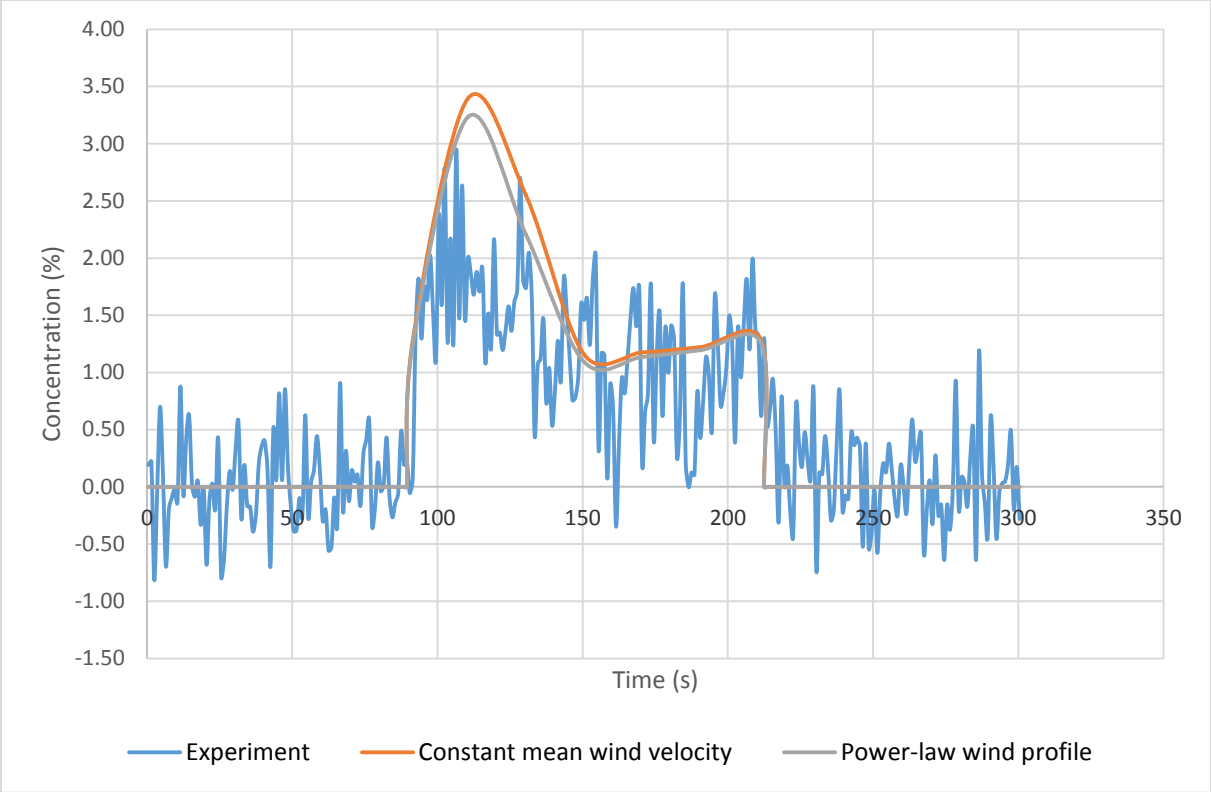

Figure 30: Concentration variations with time at 20 m downstream from release point

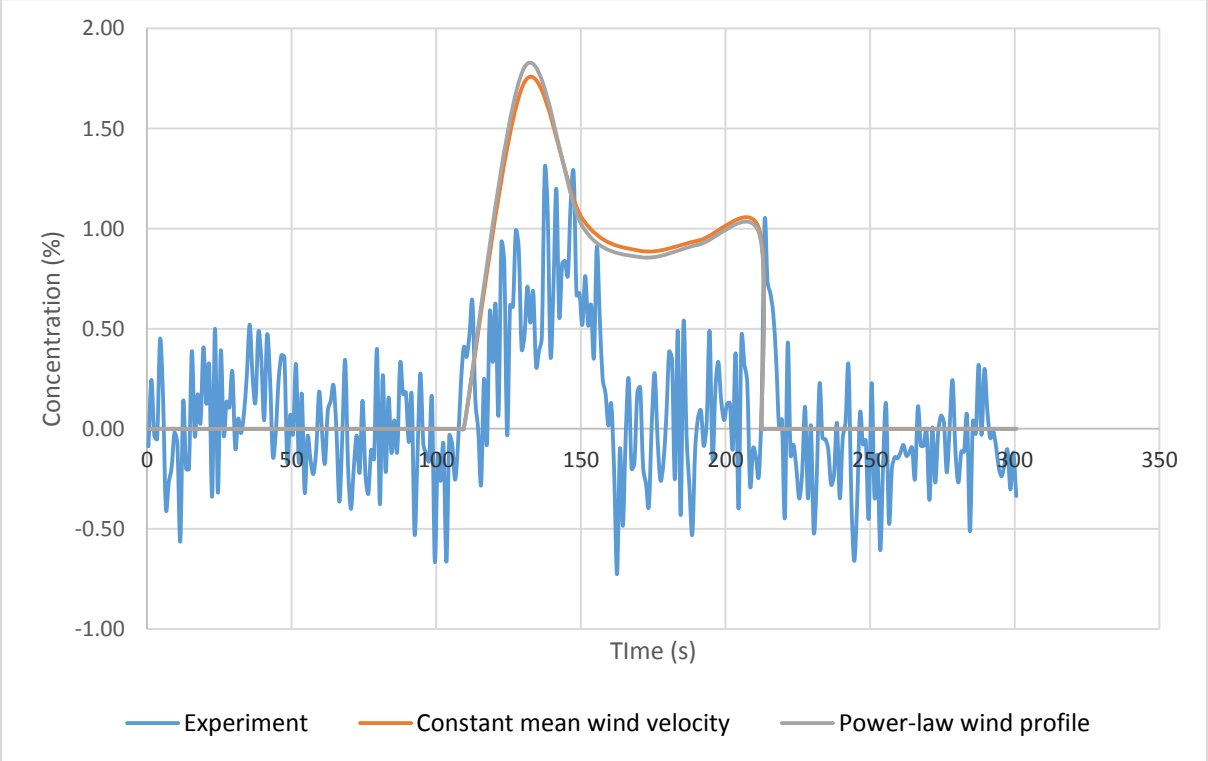

Figure 31: Concentration variations with time at 40 m downstream from release point

Table 12: Maximum concentrations reported by experiment vs FLUENT results

Distance downstream (m)	Maximum concentration (% vol) (Experiment)	Maximum concentration (% vol) (20 seconds Time averaging)- FLUENT
5	9.185	8.870
10	4.061	5.582
15	2.987	3.591
20	2.951	3.395
40	1.299	1.731

The over-prediction in peak concentration in case of 40 m downwind can be attributed to the mean wind velocity and direction fluctuations. There is no significant influence of the wind profile observed in the near-field due to relatively high jet speed near the nozzle exit leading to lesser deviations. It can be observed from figure 32 that the jet rapidly loses momentum and the jet velocity decreases and reaches a point where further flow is governed by wind velocity. The constant mean velocity during discharge in FLUENT is observed to be 7.6 m/s far-field from the release while that in case of the experiment was observed to be 6.1 m/s. Hence, these wind velocity fluctuations will lead to less accurate and over-predicted results as we progress further downwind in the far-field. Another reason for larger concentration deviations could be due to time-averaging effect. The time-average was selected sufficiently small to predict the peak concentrations but at larger distances could lead to deviations due to wind turbulence. A reduction in the time-averaging interval could give better results at far-field but would introduce turbulent fluctuations at smaller distances.

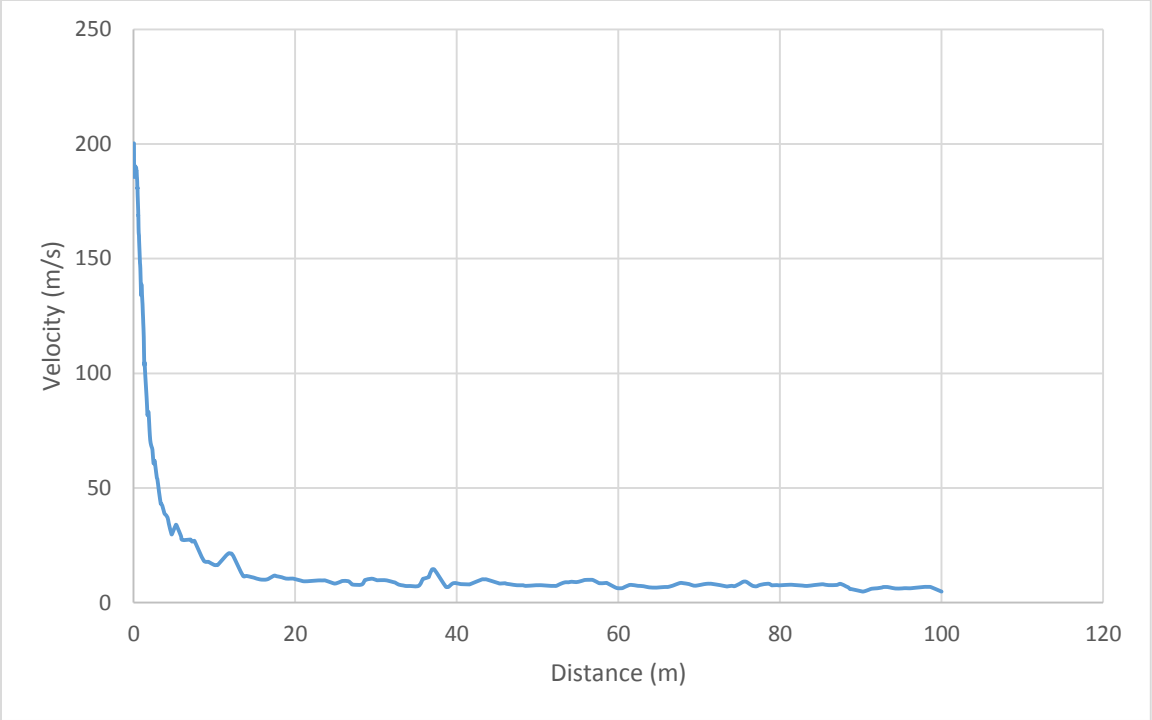

Figure 32: Velocity profile at different centerline locations downwind from the release nozzle

4.3.3 Concentration vs Distance

Figures 33 and 34 depict the concentration variations with distance at time intervals of 10 and 20 seconds, respectively. We can see that there is a rapid decrease in the concentration levels in the first few seconds of the release and thereafter, it is observed that there is a steady decrease in the concentration without many peak fluctuations.

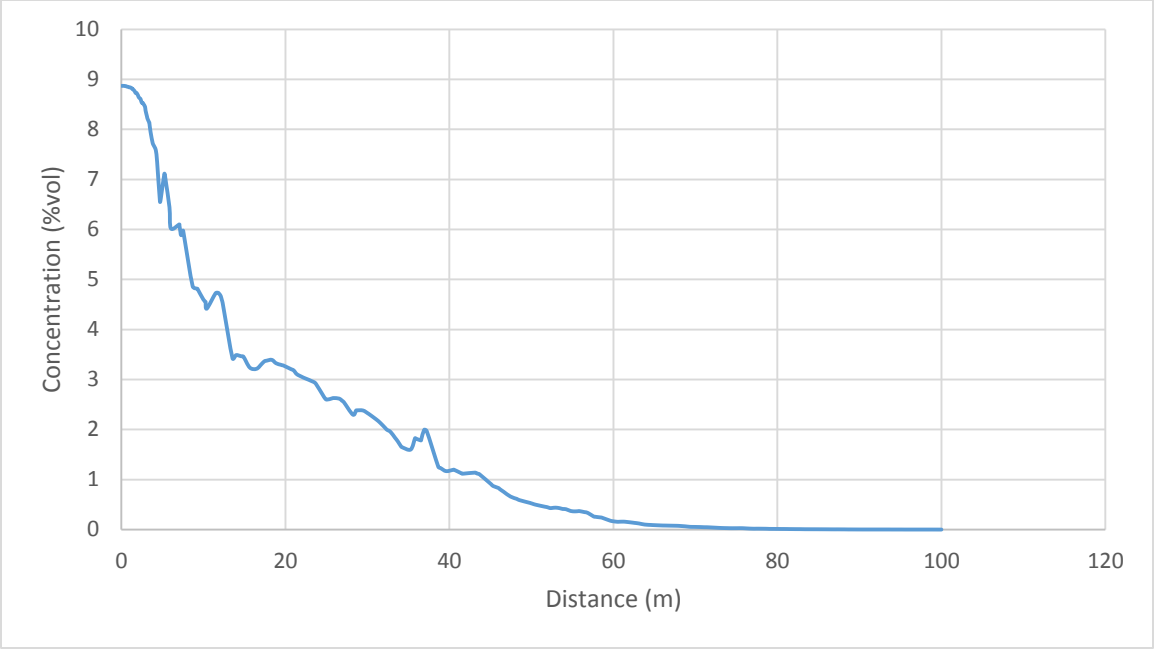

Figure 33: Concentration vs distance at 10 seconds from the release start

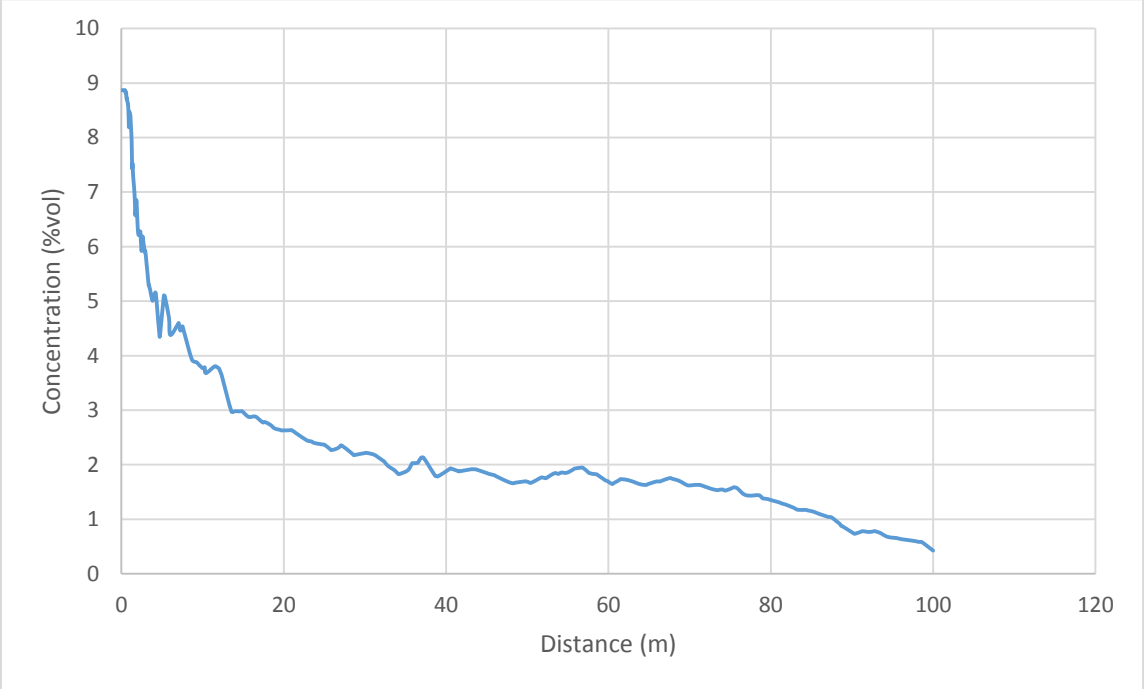

Figure 34: Concentration vs distance at 20 seconds from the release start

Figure 35 shows the concentration contours at four different time intervals of 5, 10, 15 and 20 seconds respectively. We can observe that the plume very quickly reaches a distance of

almost 100 m in the first 20 seconds. It is also observed that the CO_2 dense gas plume slumps and remains close to the ground at larger distances due to gravity, unlike other buoyant plumes which disperse in air. This is particularly due to the density differences between air and CO_2 gas. Due to this property of the gas, it is very disastrous when the pipeline runs through topographical features like valleys and depressions where the gas can accumulate and stay for extended duration leading to long lasting aftereffects.

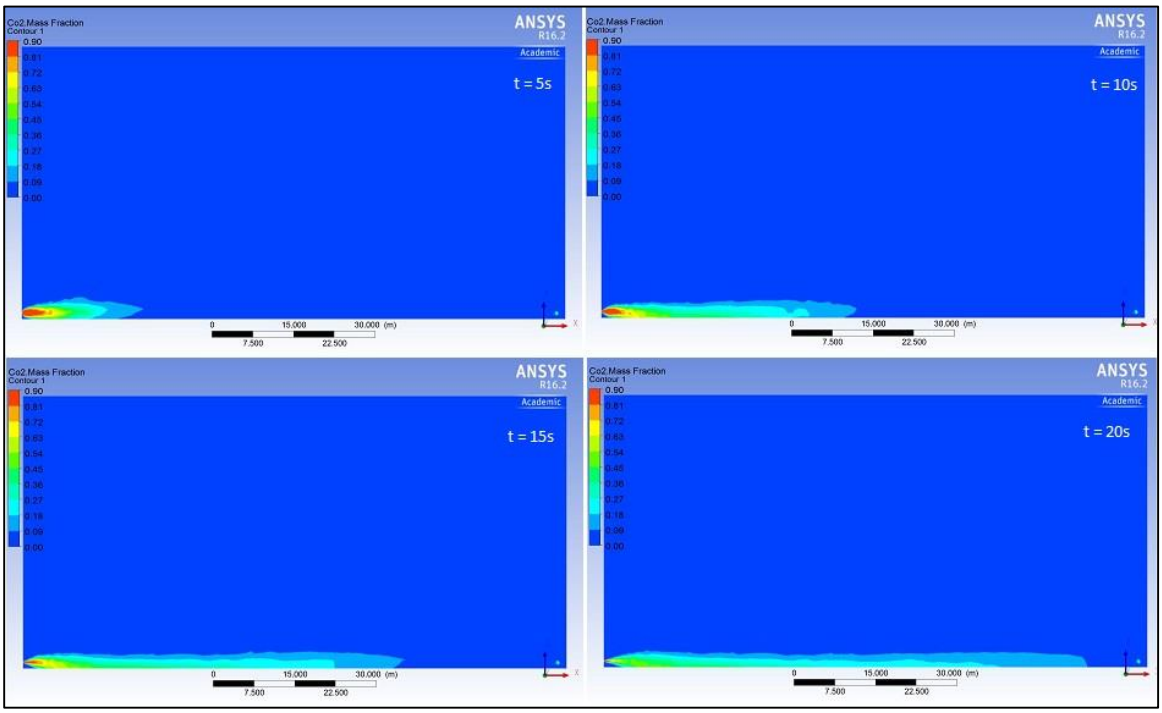

Figure 35: Concentration contours at different time intervals

Hence, Fluent can be used for determining the minimum safe distances for emergency response in an unlikely event of pipeline failure.

4.3.4 Plume Width

Figure 36 shows the snapshot of plume width spread as it expands from the nozzle exit 10 seconds after start of the leak. From the figure we can observe that the plume width is narrow

initially and almost expands to a width of 3.4 m downstream. It is observed that the maximum width of the plume reaches a value of almost 4 m at a time interval of 20 seconds post leak. As time progresses, the plume gets narrower and stays close to the ground at farther distances.

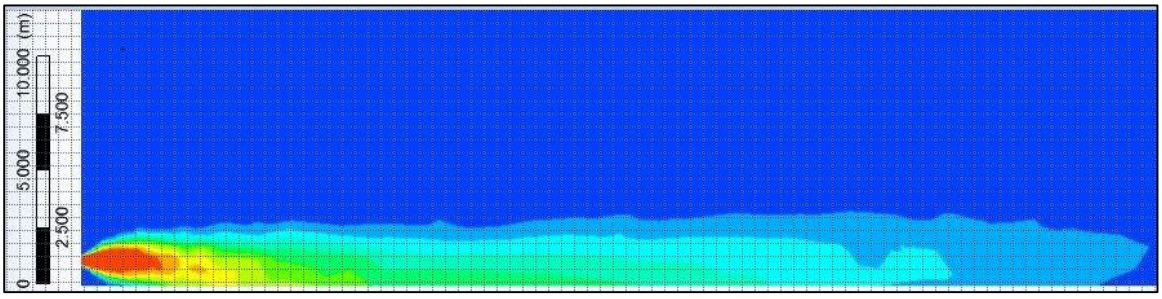

Figure 36: Plume width 10 seconds after the leak

4.3.5 Temperature Fluctuations in the Emerging Plume

To illustrate the temperature changes with respect to distance, a contour is shown for the first 5 seconds in figure 37. The plume reaches ambient temperature from a sublimation temperature of 194 K within a distance of 15 m. The plume slowly narrows down as time progresses and thereafter the temperature quickly reaches atmospheric temperature within a distance of less than 5 m.

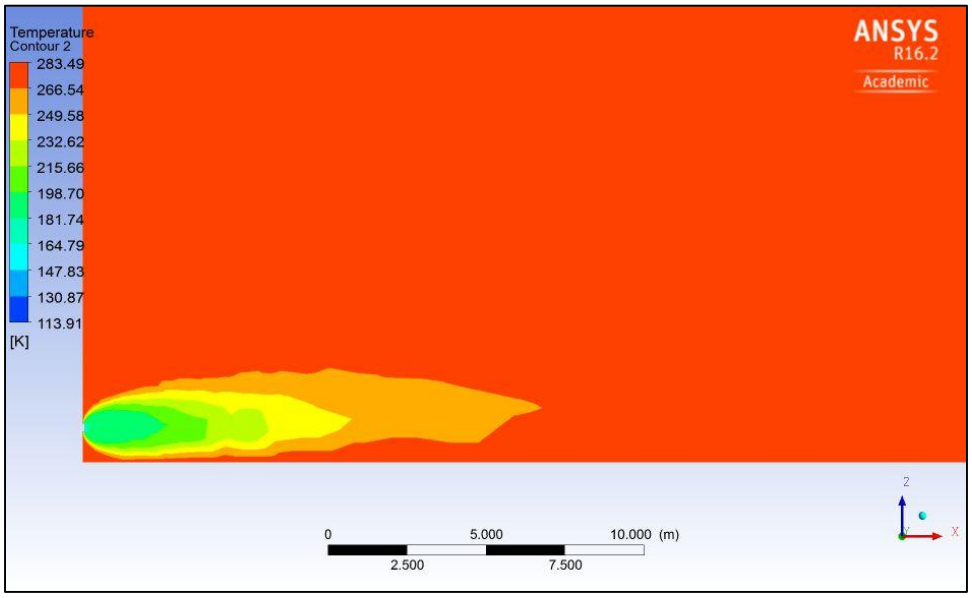

Figure 37: Temperature variation contours after 5 seconds in dispersion modeling

4.3.6 Effect of Obstacles on CO_2 Concentrations in Far-field

A case study was performed by placing obstacles that can be scaled up in actual scenario to represent buildings and tall structures. Obstacles of height 2 m were placed at distances of 8 m and 20 m from the source and a 20 seconds transient simulation was carried out to determine the effect of the dense gas plume accumulation in low-lying or topographical areas. It was observed that there is a sudden jump in the CO_2 concentration once the plume comes in contact with the obstacle at 20 m distance. A centerline concentration curve was plotted with respect to distance and it can be seen that the concentration curve decreases to a value of 3.9% at a distance of 20 m from the source but increases rapidly to a value of 5.74% due to accumulation. The concentration curve in between 20 m and 30 m is occupied by the obstacle and hence not traced in the plot below.

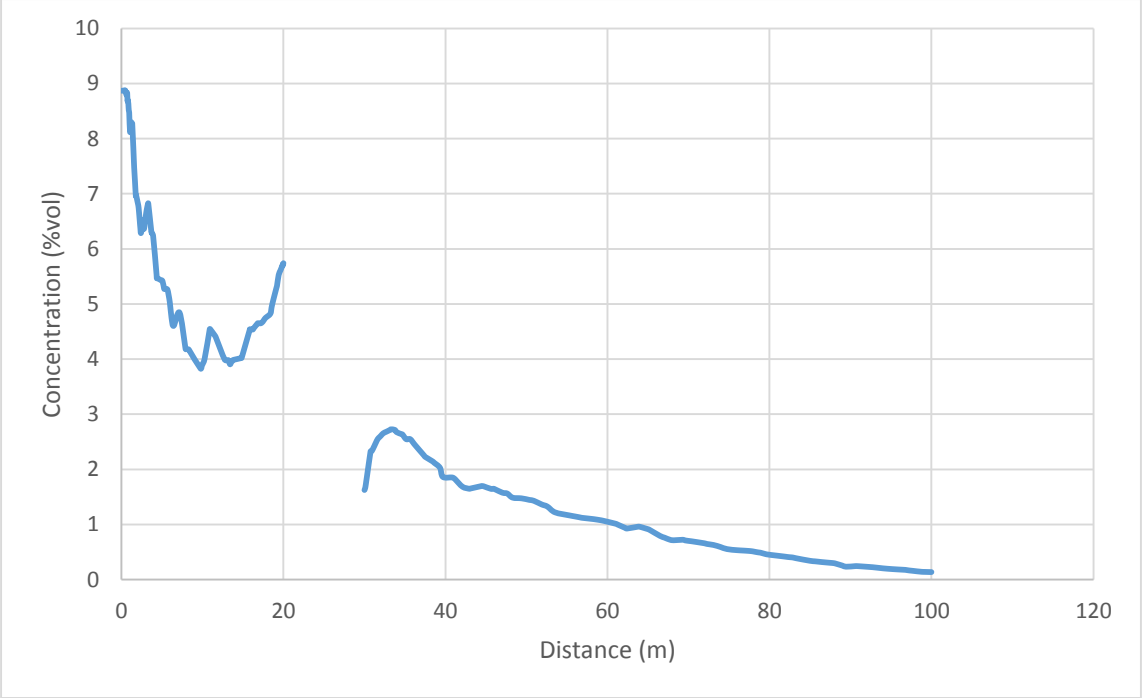

Figure 38: Centerline concentration vs distance plot in the presence of obstacles

Iso-contour of the concentration variation across the obstacles is shown in the figure 39, below. We can observe that the release impinges on the buildings and persists for some time before

it overcomes the obstacle height and spreads rapidly to larger distances downwind. The type of structure and its dimension greatly affects the concentration levels and rate of downwind dispersion.

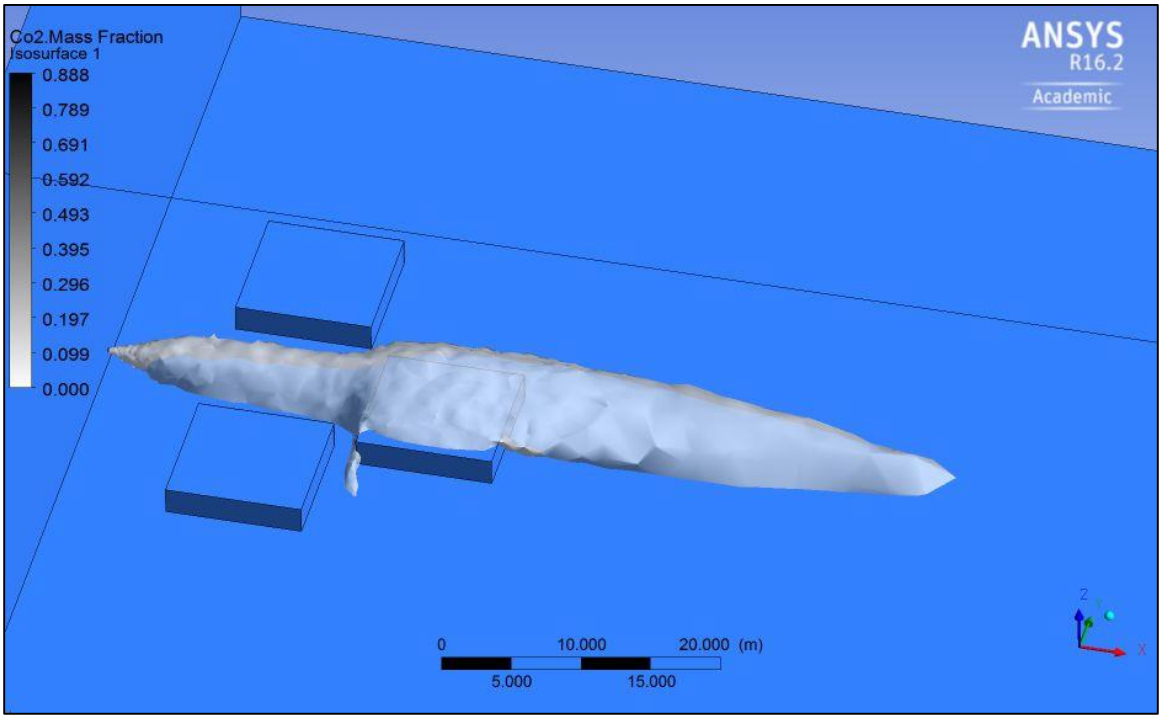

Figure 39: Iso-surface of CO_2 plume dispersion in the presence of obstacles in the first 20 seconds for concentrations up to 10,000 ppm.

CHAPTER V

CONCLUSIONS AND RECOMMENDATIONS

5.1 Conclusions

This study was aimed at understanding the complex thermodynamic behavior and leak characteristics of supercritical CO_2 in the unlikely event of sudden depressurization of the pipeline. This would be helpful for quantitative risk assessment in determining the minimum safe distances and addressing the existing knowledge gaps. A brief summary of the past failure cases was taken into consideration to determine the type (horizontal) and size of the leak (medium) which could lead to maximum damage. A two-step modeling process of determining the source strength and the further dispersion based on the pseudo-source characteristics was carried out in FLUENT 6.2 software. It was concluded based on the observations of the source term modeling that FLUENT could successfully handle the phase changes in the expansion of supercritical CO_2 to ambient conditions by accounting for the solid dry-ice formation outside the pipeline.

From the study it was concluded that the solids formed were distributed only up to a few millimeters after the leak in the depressurization zone and there were no solids formed inside the pipeline due to the high mass flow rate. This eliminates the risk of pipeline fracture propagation due to solid accumulation within the pipeline.

A study was carried out to understand the relation between the Mach disk location and the pseudo-source distance from the nozzle exit and it was observed in FLUENT that for the

given inlet conditions of pressure and temperature, the pseudo-source location was approximately 1.25 times that of the Mach disk location. This is particularly helpful when the model is a zero-dimension model, which is incapable of determining the point on the axis where the jet reaches ambient pressure conditions.

Validation of the present study was carried out against the supercritical release experiment 8 conducted by BP at Spadeadam test site. Homogenous equilibrium model gave good results in determining the source term characteristics like mass flow rate, temperature and vapor mass fraction which served as an input in dispersion model. 20 seconds time-averaging was done to avoid turbulent fluctuations in determining the mean concentrations. A good agreement was observed in the experimental and the calculated far-field concentrations up to 100 m downwind. Concentration contours were plotted to determine the variation of concentration at various distances and time intervals during the given transient release. The plume was observed to disperse up to a maximum height of 4 m from the ground at larger distances from the source.

The model was validated at two different ambient wind conditions of constant mean wind velocity (5.51 m/s) as well as wind power-law correlation to understand the effect of wind velocity and direction on the final concentrations of dispersed CO_2. It was observed that there was a very slight variation between the two models and the power-law profile gave slightly better average concentration predictions over the constant wind profile over the entire area.

A case study was carried out to study the effect of plume dispersion and concentration variations in the presence of obstacles like buildings and trees. It was observed that the dense gas plume was accumulated and caused high concentration regions near the obstacles when compared to concentrations noticed on a flat-terrain. Hence, the maximum safe distance as per FLUENT for an allowable concentration of 4% (40,000 ppm) as per the Federal occupational and health regulation (US) at the end of a 20 seconds time period is approximately 8.5 m from the source on a flat-terrain.

5.2 Recommendations

1) The CO_2 captured from the industries contains impurities like H_2S, NO_x, SO_x or water vapor which cannot be completely eliminated before transportation. Pure CO_2 dispersion was investigated in the present research for simplicity purpose. Further research could be carried out to understand the behavior of CO_2 gas dispersion and concentration distribution in the presence of impurities.
2) Although the water vapor fraction and non-vapor (solid) mass fraction in the expansion zone has been excluded due to non-significant impact on the predicted concentrations in far-field, investigation can be done to study the effect. The solid particle size is in the order of μm which can be simulated by using Lagrangian particle tracking approach.
3) The observed results give a good prediction of the concentrations as per the HEM assumption, but the actual process is non-homogenous and non-equilibrium. Hence, further research can be carried out considering the slip between the two-phase using the Homogenous Relaxation Model (HRM).

REFERENCES

Alinot, C. and C. Masson (2005). "K-Ɛ Model for the Atmospheric Boundary Layer Under Various Thermal Stratifications." Journal of Solar Energy Engineering, Transactions of the ASME 127: 438–443.

Atkins, P. W. and J. De Paula (2006). Atkins' Physical chemistry. Oxford ; New York, Oxford University Press.

Boden, T. A., G. Marland and R. J. Andres (2015). "Global, Regional, and National Fossil-Fuel CO_2 Emissions. Carbon Dioxide Information Analysis Center."

Cosham, A. and R. Eiber (2007). Fracture Control in CO_2 Pipelines. Transmission Of CO_2, H2, And Biogas Conference, Amsterdam, Netherlands.

Cumber, P. S., M. Fairweather, S. A. E. G. Falle and J. R. Giddings (November 1995). "Predictions of the Structure of Turbulent, Highly Underexpanded Jets." Journal of Fluids Engineering 117(4).

Dixon, C. and M. Hasson (2007). Calculating the Release and Dispersion of Gaseous, Liquid and Supercritical CO_2. IMechE Seminar.

Dixon, C. M., S. E. Gant, C. Obiorah and M. Bilio (2012). Validation Of Dispersion Models For High Pressure Carbon Dioxide Releases. Icheme Hazards XXIII Conference: 153-163.

DNV (2010). Design and Operation of CO_2 Pipelines. Det Norske Veritas (DNV-RP-J202).

DNV CO_2PIPETRANS Joint Industry Projects (2012). "Advantica Overview Report." 6256 (01).

Global CCS Institute (2014). CO_2 Pipeline Infrastructure Report. 2013/18.

Hanna, S., P. Drivas and J. Chang (1996). Guidelines for Use of Vapor Cloud Dispersion Models, AIChE/CCPS, New York.

HECA Project Site (2009). Carbon Dioxide Pipeline Risk Analysis. Appendix E Hydrogen Energy International LLC

Henning, D. (2013). "Innovations in CO_2 Pipeline Construction."

Hill, T. A., J. E. Fackrell, M. R. Dubal and S. M. Stiff (2011). Understanding the Consequences of CO_2 Leakage Downstream of the Capture Plant. Energy Procedia. 4: 2230-2237.

IEA (2010). "Energy Technology Perspectives " International Energy Agency Publications. Paris, France.

IEA (2010). Energy Technology Systems Analysis Programme. CO_2 Capture and Storage.

Innovation, B. C. (June 2015). "DISPERSION MODELLING TECHNIQUES FOR CARBON DIOXIDE PIPELINES IN AUSTRALIA."

IPCC "Special Report on Carbon Dioxide Capture and Storage, Transport of CO_2."

Kaushik, M., R. Kumar and H. G. (2015). "Review of Computational Fluid Dynamics Studies on Jets." American Journal of Fluid Dynamics.

Lankadasu, A., A. Tripathi, S. Saysset, A. Yackow and B. D. L. Roussiere (2015). "Numerical Modeling of Supercritical CO_2 Leaks and its Subsequent Dispersion in the Ambient Air." Procedia IUTAM 15: 49-56.

Liu, X., A. Godbole, C. Lu, G. Michal and P. Venton (2014). "Source Strength and Dispersion of CO_2 Releases from High-Pressure Pipelines: CFD Model Using Real Gas Equation of State." Applied Energy 126: 56-68.

Liu, Y.-H., G. Calvert, C. Hare, M. Ghadiri and S. Matsusaka (2012). "Size Measurement of Dry Ice Particles Produced from Liquid Carbon Dioxide." Journal of Aerosol Science 48: 1-9.

Mahgerefteh, H., S. Brown and G. Denton (2012). "Modelling the Impact of Stream Impurities on Ductile Fractures in CO_2 Pipelines." Chemical Engineering Science 74: 200-210.

Mazzoldi, A., T. Hill and J. J. Colls (2008). " CO_2 Transportation for Carbon Capture and Storage: Sublimation of Carbon Dioxide From a Dry Ice Bank." International Journal of Greenhouse Gas Control.

Mazzoldi, A. and C. M. Oldenburg (February 2013). "Leakage Risk Assessment of CO_2 Transportation by Pipeline at the Illinois Basin Decatur Project."

Mazzoldi, A., D. Picard, P. G. Sriram and C. M. Oldenburg (2013). "Simulation-Based Estimates of Safety Distances for Pipeline Transportation of Carbon Dioxide." Greenhouse Gases: Science and Technology 3(1): 66-83.

McConnell, R. A. and D. J. V. Haswell (2012). UKOPA Pipeline Product Loss Incidents and Faults Report (1962-2011), UKOPA.

NIOSH (1996). Immediately Dangerous to Life or Health Concentrations (IDLH), The National Institute for Occupational Safety and Health.

Pasquill, F. (1961). The Estimation of the Dispersion of Windborne Material. The Meteorological Magazine. 90: 33-49

Peterson, E. W. and J. P. J. Hennessey (1978). "On the Use of Power Laws for Estimates of Wind Power Potential." Journal of Applied Meteorology 17: 390–394.

Rusli, R., E. J. T. Chang, H. H. P. L. Pham and A. M. Shariff (2014). "Solid Carbon Dioxide Formation from Rapid Fluid Expansion using Integration of Computational Fluid Dynamics and Mathematical Modelling." The Italian Association of Chemical Engineering 36.

Smith, J. A. (September 2011). "CALIFORNIA POLYTECHNIC STATE UNIVERSITY WIND RESOURCE ASSESSMENT."

Span, R. and W. Wagner (1996). "A New Equation of State for Carbon Dioxide Covering the Fluid Region from the Triple Point Temperature to 1100 K at Pressures up to 800 Mpa." Journal of Physical and Chemical Reference Data: 1509-1596.

Sun, X.-Y., T.-J. Wang, Z.-W. Wang and Y. Jin (2002). "The Characteristics of Coherent Structures in the Rapid Expansion Flow of the Supercritical Carbon Dioxide." The Journal of Supercritical Fluids 24, 231-237.

U.S. Environmental Protection Agency (2016). U.S. Greenhouse Gas Inventory Report: 1990-2014. 430-R-16-002.

VDI-WA (1997). VDI-WA97, Springer Verlag, Heidelberg.

Vendrig, M., J. Spouge, A. Bird, J. Daycock and O. Johnsen (2003). Risk Analysis of the Geological Sequestration of Carbon Dioxide, Department of Trade and Industry's Cleaner Coal Technology Transfer Programme. R246 DTI/Pub URN 03/1320.

Wilcox, J. (Mar 28, 2012). "Carbon Capture." Springer Science & Business Media.

Witkowski, A., A. Rusin, M. Majkut, S. Rulik and K. Stolecka (2015). Advances in Carbon Dioxide Compression and Pipeline Transportation Processes, Springer International Publishing.

Witlox, H. W. M., M. Harper, A. Oke and J. Stene (2014). "Validation of Discharge and Atmospheric Dispersion for Unpressurised and Pressurised Carbon Dioxide Releases." Process Safety and Environmental Protection.

Witlox, H. W. M., J. Stene, M. Harper and S. H. Nilsen (2011). "Modelling of Discharge and Atmospheric Dispersion for Carbon Dioxide Releases Including Sensitivity Analysis for Wide Range of Scenarios." Energy Procedia 4: 2253–2260.

Woodward, J. L. (2010). "Estimating the Flammable Mass of a Vapor Cloud, Appendix - A." American Institute of Chemical Engineers.

Woolley, R. M., M. Fairweather, C. J. Wareing, S. A. E. G. Falle, C. Proust, J. Hebrard and D. Jamois (2013). "Experimental Measurement and Reynolds-Averaged Navier–Stokes Modelling of the Near-Field Structure of Multi-Phase CO_2 Jet Releases." International Journal of Greenhouse Gas Control 18: 139–149.

Zalosh, R. and C. W. Hung (1994). Carbon Dioxide Discharge Test Modelling. The Fourth International Symposium, Center for Fire Safety Studies.

Ansys FLUENT User's Guide, Release 15.0, Novenber 2013

APPENDIX - A

User-defined function (UDF) for wind power law correlation (Smith September 2011)

```
#include "udf.h"

#define Ur 5.2

#define Zr 5.05

DEFINE_PROFILE(x_velocity,t,i)

{

real y[ND_ND];

real z;

face_t f;

begin_f_loop(f,t)

{

F_CENTROID(y,f,t);

z = y[1];

F_PROFILE(f,t,i) = Ur*pow((z/Zr),(1./7.));

}

end_f_loop(f,t)

}
```

VITA

Preeti Joshi

Candidate for the Degree of

Master of Science

Thesis: CONSEQUENCE ANALYSIS OF THE ACCIDENTAL RELEASE OF SUPERCRITICAL CO_2 FROM HIGH PRESSURE PIPELINES

Major Field: Chemical Engineering

Biographical:

Education:

Completed the requirements for the Master of Science in Chemical Engineering at Oklahoma State University, Stillwater, Oklahoma in July, 2016.

Completed the requirements for the Bachelor of Science in Chemical Engineering at Osmania University, Hyderabad, Telangana, India in August, 2011.

Experience:
Graduate Research and Teaching Assistant, Oklahoma State University, Stillwater, OK (January 2015 – May 2016)

Professional Memberships:
Chemical Engineering Graduate Student Association - member